REPORT DOCUMENTATION PAGE

Form Approved
OMB No. 0704-0188

PLEASE DO NOT RETURN YOUR FORM TO THE ABOVE ORGANIZATION.

1. REPORT DATE *(DD-MM-YYYY)*	2. REPORT TYPE	3. DATES COVERED *(From - To)*
04-01-2008	Final	01-3-2004 to 31-03-2008

4. TITLE AND SUBTITLE

Realizing Sources for Electromagnetic Wavelets and Implementing the Wavelet Radar Concept

5a. CONTRACT NUMBER

5b. GRANT NUMBER

FA9550-04-1-0139

5c. PROGRAM ELEMENT NUMBER

6. AUTHOR(S)

Gerald Kaiser

5d. PROJECT NUMBER

5e. TASK NUMBER

5f. WORK UNIT NUMBER

7. PERFORMING ORGANIZATION NAME(S) AND ADDRESS(ES)

Center for Signals and Waves
3803 Tonkawa Trail #2
Austin, TX 78756

8. PERFORMING ORGANIZATION REPORT NUMBER

9. SPONSORING/MONITORING AGENCY NAME(S) AND ADDRESS(ES)

Dr. Arje Nachman
Air Force Office of Scientific Research
875 North Randolph St., Rm 3112
Arlington, VA 22203

10. SPONSOR/MONITOR'S ACRONYM(S)

AFOSR/NE

11. SPONSOR/MONITOR'S REPORT NUMBER(S)

12. DISTRIBUTION/AVAILABILITY STATEMENT

DISTRIBUTION A. Approved for public release; distribution unlimited.

13. SUPPLEMENTARY NOTES

14. ABSTRACT

Electromagnetic wavelets designed for applications to radar and communications have been constructed, and their charge-current sources have been computed. It has been suggested that optimal antennas for radiating and receiving such wavelets are oblate spheroidal shells.

15. SUBJECT TERMS

16. SECURITY CLASSIFICATION OF:			17. LIMITATION OF ABSTRACT	18. NUMBER OF PAGES	19a. NAME OF RESPONSIBLE PERSON
a. REPORT	b. ABSTRACT	c. THIS PAGE			Gerald Kaiser
					19b. TELEPHONE NUMBER *(Include area code)* 512-371-9424

Reset

Standard Form 298 (Rev. 8/98)
Prescribed by ANSI Std. Z39.18

FINAL REPORT

AFOSR Grant # FA9550-04-1-0139
01 March 2004 - 28 February 2007
Additional Work Effort: 01 March 2007 - 30 November 2007
No-Cost Extension: 1 December 2007 - 31 March 2008

GRANT TITLE:
Realizing Sources for Electromagnetic Wavelets and Implementing the Wavelet Radar Concept

PI Name: Gerald Kaiser
PI Address: 3803 Tonkawa Trail #2, Austin, TX 78756
PI Phone: 512-371-9424
PI Fax: 512-371-9424 (Prefer email attachments; please call to notify of fax)
PI email address: kaiser@wavelets.com

A. ORIGINAL OBJECTIVES:

1. Collaborate with with Prof. Bialynicki-Birula, who has developed a "twistorial Fourier transform" useful for generating EM and other conformal fields. We have recently discovered a close connection between this transform and EM wavelets and intend using this in several ways, including the construction of *twisted* EMW which are expected to have better collimation and stability characteristics than the present ones.
2. I have recently participated in a NATO Singular Optics workshop, where I become interested in polarization singularities and their applications to EM wavelets. I plan to study related issues of angular momentum, spin, helicity and vorticity. Some of this work may also be done jointly with Prof. Bialynicki-Birula as it is related to the twisted beams.
3. Work with Prof. Konstantin Lukin, a Noise Radar expert, I met at the above workshop, who is interested in testing experimentally various antenna designs for launching EMW using the sources I have computed.
4. I plan to participate in the Multi-scale Geometry and Analysis in High Dimensions (MGA) program at IPAM to prepare for constructing fast EM wavelet transforms based on the recently computed Fourier representation of EMW sources.
5. Design fast EM wavelet transforms using ideas and methods from MGA such as curvelets, possibly with some other participants from the MGA program.

OBJECTIVES FOR ADDITIONAL WORK EFFORT:

1. Finish the theoretical analysis of PBW antennas by constructing EM wavelets whose polarization conforms to the geometry defined by the propagation of the oblate spheroidal wave fronts. The current formulation is based on Whittaker potentials,

which have no relation to the spheroidal geometry. Finding conformal polarizations has practical consequences since it would greatly simplify the mathematical expressions for the sources, hence their implementation, and should also improve the efficiency of the antennas.
2. Collaborate with Professors Anthony Devaney and Edwin Marengo (Northeastern University) to help Dr. Richard Albanese and his team at Brooks City Base construct realizations of PBW with optimal power, energy and efficiency for the purpose of high-resolution remote sensing and imaging.

B. OBJECTIVE ADDED DURING GRANT PERIOD:
Find natural polarizations for EM wavelets that are consistent with the spheroidal geometry of the scalar pulsed-beam wavelets (PBW) used to derive the EM wavelets.

STATUS OF EFFORT
[A brief statement of progress towards achieving the research objectives. Please make this substantive (Limit to 200 words).]

1. Prof. Bialinicki-Birula's method turned out to be capable only of giving *sourceless* EM waves, which rules out its applicability to the production of EM wavelets. However, I developed an independent method for constructing EM wavelets with arbitrary angular momentum about the beam axis. See the attached papers *Retarded multipole wavelets* Parts I and II.
2. Prof. Lukin visited me in July 2005 and his efforts culminated in a report (attached), but Dr. Albanese and I concluded this had limited value.
3. The collaboration with Profs. Devaney and Marengo resulted in a significant paper (attached), to appear in IEEE Transactions in Antennas & Propagation, which validates the realizability and usefulness of EM wavelets.
4. The method of Debye potentials (suggested by Prof. Devaney) yields EM wavelets whose polarizations are consistent with the spheroidal geometry of the scalar PBW. I believe all the elements are now in place for the realization and fabrication of EM wavelet sources.

ACCOMPLISHMENTS/NEW FINDINGS
[Describe research highlights, their significance to the field, their relationship to the original goals, their relevance to the AF's mission, and their potential applications to AF and civilian technology challenges.]

1. The singular pulsed-beam wavelet sources, supported on disks, have been replaced by equivalent *shell sources* supported on spheroidal surfaces or shells surrounding the disks.

2. This method was recently found to yield a conserved transmission current which expresses the invariance of the transmission amplitude between wavelet sources with respect to deformation of the equivalent source.

PERSONNEL SUPPORTED

[List professional personnel supported by and/or associated with the research effort.]

1. Prof. Konstantin Lukin
   National Academy of Sciences of Ukraine
   Institute of Radiophysics and Electronics
   Kharkov, Ukraine
   Consulting on wavelet antenna fabrication
   Total of 100 hours at $40/hour

2. David Park
   5605 West Falls Road
   Mount Airy, MD 21771
   Mathematica programming & graphics consulting
   Total of 20 hours at $40/hour

PUBLICATIONS

[List peer-reviewed publications submitted and/or accepted during the 12-month period starting the previous 1 August (or since start for new grants).]

1. G. Kaiser, *Helicity, polarization, and Riemann-Silberstein vortices.* Journal of Optics A, Pure Appl. Opt. 6 (2004) S243–S245.
2. G. Kaiser, *Energy-momentum conservation in pre-metric electrodynamics with magnetic charges.* J. Phys. A: Math. Gen. 37 (2004) 7163 - 7168.
3. G. Kaiser, *Making electromagnetic wavelets.* J. Phys. A: Math. Gen. 37 (2004) 5929 - 5947.
4. G. Kaiser, *Distributional sources for Newman's holomorphic Coulomb fields.* J. Phys. A: Math. Gen. 37 (2004) 8735 - 8745.
5. G. Kaiser, Eigenwavelets of the Wave equation. In *Harmonic Analysis, Signal Processing, and Complexity,* I. Sabadini, D.C. Struppa and D.F. Walnut, editors, Birkhauser, 2005, pages 121 - 134.
6. G. Kaiser, *Making electromagnetic wavelets II: Spheroidal shell antennas.* J. Phys. A: Math. Gen. 38 (2005) 495 - 508.
7. G. Kaiser, *Pulsed-Beam Wavelets and Wave Equations.* IMA Workshop on Imaging from Wave Propagation, Minneapolis, MN, October 17-21, 2005.
8. G. Kaiser, *Analytic Pulsed-Beam Communication Channels.* PIERS 2006, Cambridge, MA, March 26-29, 2006.

9. G. Kaiser, *Electromagnetic wavelets as Hertzian pulsed beams in complex spacetime.* Invited chapter in *Topics in Mathematical Physics General Relativity and Cosmology,* Festschrift in Honor of Jerzy Plebanski. H. Garcia-Compean, B. Mielnik, M. Montesinos and M. Przanowski (Editors). World Scientific, 2006.
10. G. Kaiser, *Extended wave propagators as pulsed-beam communication channels.* Days on Diffraction 06 Proceedings, 2007.
11. A.J. Devaney, G. Kaiser, E.A. Marengo, R. Albanese, G. Erdmann, *The Inverse Source Problem for Wavelet Fields.* Accepted for publication by IEEE Transactions in Antennas & Propagation.
12. G. Kaiser, *Screened sources and conserved transmission currents.* In preparation.

BOOK IN PREPARATION (6 of 12 chapters completed):
Communication with Electromagnetic Wavelets, under contract for
Progress in Mathematical Physics book series, Birkhauser-Boston.

INTERACTIONS/TRANSITIONS
Participation/Presentations At Meetings, Conferences, Seminars, Etc.
[Be selective, but be sure to include participations that reflect the quality/impact of the effort]

A. Conferences:
1. Invited lecture, conference in honor of Carlos Berenstein, George Mason University, May 17-20, 2004.
2. Plenary lecture, 7th International Conference on Clifford Algebras, Toulouse, France, May 19-29, 2005
3. Plenary lecture, *Days on Diffraction*, St. Petersburg, Russia, May 30-June 2, 2006.
4. Kaiser, *Screened sources and conserved transmission currents.* In preparation.

B. Seminars & Lectures:
1. *Making electromagnetic wavelets.* Physics department colloquium, University of Texas, March 10, 2004.
2. *Making electromagnetic wavelets.* ICES & CAM Seminar, University of Texas, April 19, 2004.
3. *Making electromagnetic wavelets.* GM Wireless Networking and Communications Seminar, University of Texas, April 30, 2004.
4. *Realizable sources for electromagnetic wavelets.* 3M Campus, Austin, TX, April 13, 2005.
5. *Small Radiators for electromagnetic wavelets.* ACM Colloquium, Caltech, April 25, 2005.
6. *Extended wave propagators as pulsed-beam communication channels.* Mathematical Physics Seminar, Univedrsity of Texas at Austin, November 11, 2005.

7. *Making electromagnetic wavelets*. Mathematics Colloquium, University of Texas at San Antonio, March 28, 2008.

* Consultative And Advisory Functions To Other Laboratories And Agencies
[Consultative and advisory functions to other laboratories and agencies, especially Air Force and other DoD laboratories. Provide factual information about the subject matter, institutions, locations, dates, and name(s) of principal individuals involved.]

Beginning in October 2007, I have been giving 3-hour monthly lectures on EM wavelets and the underlying mathematics at Brooks City Base in San Antonio, TX. The audience has consisted of Drs. Albanese, Grant Erdmann, Sherwood Samn (all at Brooks), Prof. Walter Richardson (UTSA) and several others.

NEW DISCOVERIES, INVENTIONS, OR PATENT DISCLOSURES
[If none, report None.]

None.

INSTITUTE OF PHYSICS PUBLISHING JOURNAL OF PHYSICS A: MATHEMATICAL AND GENERAL

J. Phys. A: Math. Gen. **37** (2004) 5929–5947 PII: S0305-4470(04)76781-5

Making electromagnetic wavelets

Gerald Kaiser

Center for Signals and Waves, 3803 Tonkawa Trail #2, Austin, TX 78756-3915

E-mail: kaiser@wavelets.com

Received 26 February 2004
Published 18 May 2004
Online at stacks.iop.org/JPhysA/37/5929
DOI: 10.1088/0305-4470/37/22/015

Abstract

Electromagnetic wavelets are constructed using scalar wavelets as superpotentials, together with an appropriate polarization. It is shown that *oblate spheroidal antennas*, which are ideal for their production and reception, can be made by deforming and merging two branch cuts. This determines a unique field on the interior of the spheroid which gives the boundary conditions for the surface charge-current density necessary to radiate the wavelets. These sources are computed, including the *impulse response* of the antenna.

PACS numbers: 02.30.Jr, 02.30.Uu, 41.20.Jb, 41.85.Ct

1. Complex distance and its branch cuts

Electromagnetic wavelets were introduced in [K94] as localized solutions of Maxwell's equations. They are 'wavelets' in the historical sense of Huygens as well as the modern one: being generated from a single 'mother wavelet' by conformal transformations including translations and scaling, they form *frames* that provide analysis-synthesis schemes for general electromagnetic waves. Together with their scalar (acoustic) counterparts, they have been called *physical wavelets*. It was pointed out that they can, in principle, be emitted and absorbed causally, and applications to radar and communications have been proposed [K96, K97, K1] based on their remarkable ability to focus sharply and without sidelobes. Similar objects, long studied in the engineering literature under the name *complex-source pulsed beams*, have been used to build beam summation methods and analyse the behaviour of solutions (see [HF1] for a recent review). However, to implement the proposed applications to radar and communications, the wavelets must be *realized* by simulating their *sources*. This has proved to be difficult, and detailed investigations have only been made recently [HLK0, K3]. Here I present a new and rather complete analysis of the sources based on an insight which I believe is a key to their realization: *the sources can be constructed from the very branch cuts that give the wavelets their remarkable properties*.

Physical wavelets are based on the idea of displacing a point source to *complex coordinates*. Since a *real* translation gives nothing new, it suffices to discuss a point source with purely imaginary coordinates $\mathrm{i}\boldsymbol{a}$. It will be seen that this results in a *real, coherent, extended source distribution* parametrized by the single vector $\boldsymbol{a}$, much as an antenna dish can be described by a single vector giving the orientation and radius of the dish.

Recall the definition of the *complex distance* σ from the imaginary source point $\mathrm{i}\boldsymbol{a}$ to the real field point $\boldsymbol{r}$,

$$\sigma(\boldsymbol{r} - \mathrm{i}\boldsymbol{a}) = \sqrt{(\boldsymbol{r} - \mathrm{i}\boldsymbol{a}) \cdot (\boldsymbol{r} - \mathrm{i}\boldsymbol{a})} = \sqrt{r^2 - a^2 - 2\mathrm{i}\boldsymbol{a} \cdot \boldsymbol{r}}. \tag{1}$$

For each fixed source location $\mathrm{i}\boldsymbol{a} \neq \boldsymbol{0}$, its branch points form a circle:

$$\sigma = 0 \Rightarrow \boldsymbol{r} \in \mathcal{C} = \{\boldsymbol{r} \in \mathbb{R}^3 : r = a, \boldsymbol{a} \cdot \boldsymbol{r} = 0\}.$$

It is important to note the *topological* difference between $\boldsymbol{a} \neq \boldsymbol{0}$, when $\mathbb{R}^3 - \mathcal{C}$ is multiply connected, and $\boldsymbol{a} = \boldsymbol{0}$, when $\mathcal{C}$ contracts to the origin and $\mathbb{R}^3 - \mathcal{C}$ becomes simply connected. Writing

$$\sigma = p - \mathrm{i}q \tag{2}$$

note that (1) implies

$$r^2 - a^2 = p^2 - q^2 \qquad \boldsymbol{a} \cdot \boldsymbol{r} = pq$$

from which one easily obtains the relations to the cylindrical coordinates with z-axis parallel to $\boldsymbol{a}$:

$$az = pq \qquad a\rho = a\sqrt{r^2 - z^2} = \sqrt{p^2 + a^2}\sqrt{a^2 - q^2}. \tag{3}$$

This gives an important bound on the 'complexness' of σ in terms of the 'complexness' of its argument:

$$|q| \leqslant a \qquad \text{or} \quad |\mathrm{Im}\,\sigma(\boldsymbol{z})| \leqslant |\mathrm{Im}\,\boldsymbol{z}| \qquad \boldsymbol{z} = \boldsymbol{r} - \mathrm{i}\boldsymbol{a}.$$

It follows from (3) that

$$\frac{\rho^2}{a^2 + p^2} + \frac{z^2}{p^2} = \frac{\rho^2}{a^2 - q^2} - \frac{z^2}{q^2} = 1$$

hence the level surfaces of p^2 form a family of *oblate spheroids*

$$\mathcal{S}_p = \{\boldsymbol{r} : p^2 = \text{const} > 0\} = \left\{\boldsymbol{r} : \frac{\rho^2}{a^2 + p^2} + \frac{z^2}{p^2} = 1\right\} \tag{4}$$

and those of q^2 form the orthogonal family of one-sheeted *hyperboloids*

$$\mathcal{H}_q \equiv \{\boldsymbol{r} : 0 < q^2 = \text{const} < a^2\} = \left\{\boldsymbol{r} : \frac{\rho^2}{a^2 - q^2} - \frac{z^2}{q^2} = 1\right\}. \tag{5}$$

To complete the picture, we include the following *degenerate* members of these families,

$$\mathcal{S}_0 = \{\boldsymbol{r} : 0 \leqslant \rho \leqslant a, z = 0\} \tag{6}$$

$$\mathcal{H}_0 = \{\boldsymbol{r} : a \leqslant \rho < \infty, z = 0\}$$

$$\mathcal{H}_a = \{\boldsymbol{r} : \rho = 0, -\infty < z < \infty\} \tag{7}$$

where $\mathcal{S}_0$ and $\mathcal{H}_0$ each form a twofold cover of the indicated sets.

The families $\mathcal{S}_p$ and $\mathcal{H}_q$ are depicted in figure 1, along with the azimuthal half-plane $\phi = \text{constant}$. They are *confocal*, with the branch circle $\mathcal{C}$ as their common focal set. Note that the intersection of $\mathcal{S}_p$ with $\mathcal{H}_q$ consists of two circles whose further intersection with the

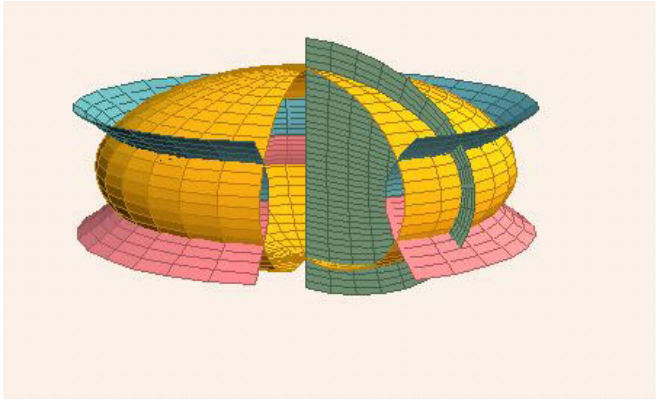

Figure 1. The level surfaces of σ form an oblate spheroidal coordinate system.

azimuthal half-plane consist of two points for each choice of (p^2, q^2, ϕ). When $p = q = 0$, the two circles merge with the branch circle $\mathcal{C}$. The set of numbers

$$(\sigma, \phi) \equiv (p, q, \phi) \qquad -\infty < p < \infty \qquad -a \leqslant q \leqslant a \qquad 0 \leqslant \phi < 2\pi$$

therefore gives a *twofold cover* of $\mathbb{R}^3 - \mathcal{C}$. To obtain a coordinate system, we must choose between the two covers, and this amounts to choosing a *branch cut* that makes σ single valued, as explained below. This will result in a one-to-one correspondence between (σ, ϕ) and points $\boldsymbol{r} \in \mathbb{R}^3$ not on the branch cut, giving an *oblate spheroidal coordinate system*.

If we continue σ analytically around a closed loop threading the branch circle $\mathcal{C}$, it returns with its sign reversed. To make it single valued, it is therefore necessary to choose a branch cut that prevents the completion of the loop. Note from (1) that

$$r \gg a \Rightarrow \sigma \approx \pm(r - \mathrm{i}a\cos\theta). \tag{8}$$

The spatial region with $r \gg a$ will be called the *far zone* (we need $a > 0$ here to set the scale). Since we want σ to generalize the usual positive distance r, we insist that

$$r \gg a \Rightarrow p \approx r \qquad q \approx a\cos\theta. \tag{9}$$

If follows from (9) that the branch cut $\mathcal{B}$ is *bounded* since it must be entirely contained inside any spheroid $\mathcal{S}_p$ with p^2 sufficiently large, and its boundary must be the branch circle:

$$\partial\mathcal{B} = \mathcal{C}. \tag{10}$$

(The alternative is a branch cut extending from $\mathcal{C}$ to infinity, but this violates (9).) $\mathcal{B}$ is therefore a *membrane spanning* $\mathcal{C}$, and *any* such membrane will do. The situation is best understood topologically. The analytic continuation of the distance has opened up a window connecting the two branches of $r = \sqrt{\boldsymbol{r}\cdot\boldsymbol{r}}$, thus making $\mathbb{R}^3 - \mathcal{C}$ multiply connected. The spherical coordinates r and θ merge analytically into σ, which is double valued, and the choice of a branch cut $\mathcal{B}$ makes $\mathbb{R}^3 - \mathcal{B}$ simply connected and σ single valued.

Let σ_0 denote the complex distance with the flat disc $\mathcal{S}_0$ as branch cut:

$$\sigma_0 = p_0 - \mathrm{i}q_0 \qquad p_0 \geqslant 0 \qquad -a \leqslant q_0 \leqslant a. \tag{11}$$

The complex distance $\sigma_{\mathcal{B}}$ with $\mathcal{B}$ as branch cut is now defined as follows. Choose an arbitrary reference point $\boldsymbol{r}_0$ in the far zone, where $\sigma_{\mathcal{B}} = \sigma_0$. To find $\sigma_{\mathcal{B}}$ at any other point $\boldsymbol{r}$, continue analytically along an arbitrary path from $\boldsymbol{r}_0$ to $\boldsymbol{r}$, with the following rule: *whenever the path crosses* $\mathcal{B}$, $\sigma_{\mathcal{B}}$ *changes sign*. This gives a unique definition of $\sigma_{\mathcal{B}}$, and both $p_{\mathcal{B}}$ and $q_{\mathcal{B}}$ have a jump discontinuity across the interior of $\mathcal{B}$. Of course, $\sigma_{\mathcal{B}} = \sigma_0 = 0$ on $\mathcal{C}$.

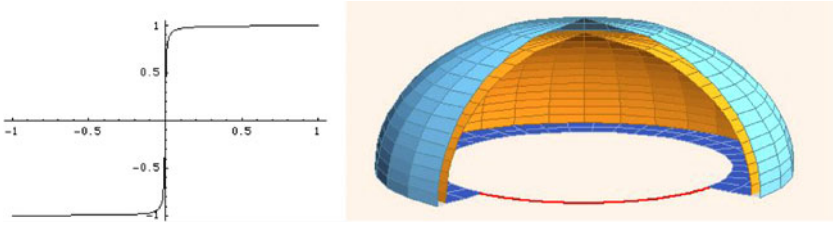

Figure 2. The cut function $\chi(q) = X_\varepsilon(q)$ with $\varepsilon = 0.005$ and its branch cut with $a = 1$. The two sheets have been purposely separated to show the double cover.

A general branch cut can be specified by a function $\chi(p, \phi)$ as

$$\mathcal{B} = \{\boldsymbol{r} \in \mathbb{R}^3 : p = \chi(q, \phi), -a \leqslant q \leqslant a, 0 \leqslant \phi \leqslant 2\pi\}, \tag{12}$$

where the *cut function* χ must satisfy

$$\chi(-q, \phi) = -\chi(q, \phi) \qquad \chi(q, 2\pi) = \chi(q, 0). \tag{13}$$

The first condition ensures that σ changes sign across $\mathcal{B}$, while the second ensures that it is continuous across the half-plane $\phi = 0$ on each side of $\mathcal{B}$. Note that $\mathcal{B}$ need not be cylindrically symmetric. We will be especially interested in the cuts $\mathcal{B}_\alpha$ defined by the cylindrical cut functions

$$\chi_\alpha(q) = \alpha \operatorname{Sgn}(q). \tag{14}$$

Note that on $\mathcal{B}_\alpha$ we have

$$az = pq = \alpha q \operatorname{Sgn}(q) = \alpha |q|.$$

If $\alpha > 0$, then the values $q \neq 0$ generate the *upper spheroid*

$$\mathcal{S}_\alpha^+ = \{\boldsymbol{r} \in \mathcal{S}_\alpha : z > 0\}.$$

But this does not include the branch circle $\mathcal{C}$, so the bounding condition (10) is not satisfied. The problem is that $\operatorname{Sgn}(q)$ is undefined at $q = 0$, and the set of all points with $q = 0$ is the degenerate hyperboloid $\mathcal{H}_0$ (7). Hence we *define* the part of $\mathcal{B}_\alpha$ with $q = 0$ as the *apron* bridging the gap between $\mathcal{C}$ and $\mathcal{S}_\alpha^+$,

$$\mathcal{B}_\alpha^0 = \{\boldsymbol{r} : a \leqslant \rho \leqslant \sqrt{a^2 + \alpha^2}, z = 0\}.$$

Thus, for $\alpha > 0$, $\chi_\alpha(q)$ defines the *upper spheroidal branch cut*

$$\mathcal{B}_\alpha = \mathcal{S}_\alpha^+ \cup \mathcal{B}_\alpha^0 \qquad \partial\mathcal{B}_\alpha = \mathcal{C}. \tag{15}$$

Similarly, $\chi_{-\alpha}(q)$ defines the *lower spheroidal cut*

$$\mathcal{B}_{-\alpha} = \mathcal{S}_\alpha^- \cup \mathcal{B}_\alpha^0 \qquad \partial\mathcal{B}_{-\alpha} = \mathcal{C}. \tag{16}$$

As $\alpha \to 0$, both cuts contract to the doubly covered flat disc spanning $\mathcal{C}$, which is the degenerate spheroid $\mathcal{S}_0$ (6).

Every branch cut $\mathcal{B}$ is doubly covered. Consider any simply connected, closed surface $\mathcal{S}$ containing $\mathcal{C}$ in its interior. Think of $\mathcal{S}$ as a balloon and of $\mathcal{C}$ as a rigid wire ring. Now *deflate* the balloon, and you have a branch cut bounded by $\mathcal{C}$. In particular, if we take $\mathcal{S} = \mathcal{S}_\alpha$ and keep the upper spheroid rigid while deflating, the balloon stretches around the ring to cover the underside of $\mathcal{S}_\alpha^+$ and we obtain the cut (15) (see figure 2).

The image of a branch cut as a balloon enclosing the singular ring is similar to Penrose's idea of *cosmic censorship* in general relativity [W99, chapter 5] where a *horizon* ($\mathcal{S}$) prevents the outside observer from seeing a *naked singularity* ($\mathcal{C}$). In light of the connection with

Newman's analytic Coulomb field (see the discussion below (54)), the two may in fact be closely related.

The discontinuity of χ_α in (14) causes two problems: the $q = 0$ contribution is undefined (hence the aprons $\mathcal{B}^0_\alpha$ had to be chosen 'by hand'), and the resulting cut had a sharp edge. For computational purposes, it may be better to use smooth cut functions to avoid both problems. Let $\varepsilon > 0$ and define

$$X_\varepsilon(q) = \frac{1}{\pi}\mathrm{Im}\ln\left(\frac{\varepsilon + \mathrm{i}q}{\varepsilon - \mathrm{i}q}\right) \qquad \chi(q) = \alpha X_\varepsilon(q). \tag{17}$$

For $\varepsilon \ll a$, $X_\varepsilon(q)$ is a smoothed version of $\mathrm{Sgn}(q)$ and the resulting branch cut closely approximates $\mathcal{B}_\alpha$ without the need to define the apron separately. This is shown in figure 2.

2. Scalar wavelets

For any fixed choice of branch cut $\mathcal{B}$, we now denote the complex distance simply by σ. Scalar wavelets are then defined as the *retarded* solutions

$$\Psi(\boldsymbol{z}, \tau) = \frac{g(\tau - \sigma)}{\sigma} \equiv \frac{g_r}{\sigma} \qquad \boldsymbol{z} = \boldsymbol{r} - \mathrm{i}\boldsymbol{a} \qquad \tau = t - \mathrm{i}b \tag{18}$$

where we have set the propagation speed $c = 1$ (otherwise $g_r = g(\tau - \sigma/c)$) and g is the *analytic-signal transform* of a driving signal $g_0(t)$, defined[1] as the convolution of g_0 with the Cauchy kernel:

$$\begin{aligned} g(\tau) &= \frac{1}{2\mathrm{i}\pi}\int_{-\infty}^{\infty}\frac{g_0(t')\,\mathrm{d}t'}{\tau - t'} \qquad \tau = t - \mathrm{i}b \\ &= \frac{b}{2\pi}\int_{-\infty}^{\infty}\frac{g_0(t')\,\mathrm{d}t'}{(t'-t)^2 + b^2} + \frac{\mathrm{i}}{2\pi}\int_{-\infty}^{\infty}\frac{(t'-t)g_0(t')\,\mathrm{d}t'}{(t'-t)^2 + b^2} \\ &= g_1(t, b) + \mathrm{i}g_2(t, b). \end{aligned} \tag{19}$$

$g_1(t, b)$ and $g_2(t, b)$ are smoothed versions of $\frac{1}{2}g_0(t)$ and its *Hilbert transform*, with b as the smoothing parameter. We assume that $g_0(t)$ decays at infinity, from which it follows that $g(\tau)$ is analytic in the upper and lower complex time half-planes $\mathbb{C}^\pm$. The original driving signal can be recovered as the boundary value

$$g_0(t) = \lim_{b\to+0}\left[g(t - \mathrm{i}b) - g(t + \mathrm{i}b)\right].$$

(The limit of the *sum* gives the Hilbert transform.) In particular, if g_0 vanishes on *any* open interval I, this interval becomes a window between the upper and lower half-planes through which the functions $g(t \pm \mathrm{i}b)$ can be connected so that they are both part of a *single* analytic function. (This is a special case of the *edge of the wedge theorem* in higher dimensions; see [K3].) Since every practical driving signal vanishes at least in the remote past, this property will be assumed. Note that this excludes time-harmonic driving signals, which are however idealizations.

Now consider the numerator of (18),

$$g(\tau - \sigma) = g(t - p - \mathrm{i}(b - q)).$$

Suppose that $|b| \leqslant a$. Then $g(\tau - \sigma)$ is undefined along the semi-hyperboloid where $q(\boldsymbol{r}) = b$, *except* when $t - p(\boldsymbol{r})$ is in the zero-set of g_0. On the other hand, if $|b| > a$, then $b - q(\boldsymbol{r})$ vanishes nowhere and $g(\tau - \sigma)$ is analytic at all $(\boldsymbol{r}, t)$. Therefore we assume from now on that

$$|b| > a \tag{20}$$

[1] This is a special case of a multidimensional definition; see [K3].

so that $g(\tau - \sigma)$ is defined unambiguously everywhere. The imaginary source coordinates must therefore belong either to the *future cone* or to the *past cone* of spacetime,

$$b > a \Rightarrow (\boldsymbol{a}, b) \in V_+ \qquad b < -a \Rightarrow (\boldsymbol{a}, b) \in V_-$$

which means that the complex 4-vector from the source point $\mathrm{i}y = \mathrm{i}(\boldsymbol{a}, b)$ to the field point $x = (\boldsymbol{r}, t)$ belongs either to the *forward tube* or the *backward tube* of complex spacetime [SW64, K3],

$$\mathcal{T}_\pm = \{z = x - \mathrm{i}y \in \mathbb{C}^4 : y \in V_\pm\} \qquad x = (\boldsymbol{r}, t) \qquad y = (\boldsymbol{a}, b). \tag{21}$$

The source distribution of Ψ is now *defined* as a generalized function by applying the wave operator,

$$S(z) = \left(\partial_t^2 - \nabla^2\right)\Psi(z) = \Box_x \Psi(z), \tag{22}$$

where $\Box_x$ indicates that the operator acts only on the real spacetime variables x of the field point. It is well known that

$$\Box \frac{h(t-r)}{r} = 4\pi h(t)\delta(\boldsymbol{r}) \tag{23}$$

for any differentiable function h, and this can be extended to $\Psi(z)$. Since Ψ is differentiable in $\boldsymbol{r}$ everywhere outside of the branch cut $\mathcal{B}$, (23) suggests that S is a (Schwartz) *distribution supported on* $\mathcal{B}$, a conclusion borne out by a rigorous analysis [K3]. The discontinuity of Ψ across $\mathcal{B}$ gives a combination of *simple and double layer* terms of S on $\mathcal{B}$ [K3].

The frequency content of $g(\tau)$ determines that of Ψ and should therefore be understood. Substituting the Fourier representation of g_0 into the definition (19) and reversing the order of integration give

$$\begin{aligned} g(\tau) &= \frac{1}{2\mathrm{i}\pi}\int_{-\infty}^{\infty}\frac{\mathrm{d}t'}{\tau - t'}\int_{-\infty}^{\infty}\frac{\mathrm{d}\omega}{2\pi}\hat{g}_0(\omega)\,\mathrm{e}^{-\mathrm{i}\omega t'} \\ &= \int_{-\infty}^{\infty}\frac{\mathrm{d}\omega}{2\pi}\hat{g}_0(\omega)\frac{1}{2\mathrm{i}\pi}\int_{-\infty}^{\infty}\frac{\mathrm{e}^{-\mathrm{i}\omega t'}\,\mathrm{d}t'}{\tau - t'}. \end{aligned} \tag{24}$$

The contour in the second integral can be closed in the lower half-plane if $b > 0$ and in the upper half-plane if $b < 0$, giving

$$g(\tau) = \mathrm{Sgn}(b)\int_{-\infty}^{\infty}\frac{\mathrm{d}\omega}{2\pi}\hat{g}_0(\omega)\Theta(\omega b)\,\mathrm{e}^{-\mathrm{i}\omega\tau} \qquad \tau = t - \mathrm{i}b \tag{25}$$

where $\Theta(\omega b)$ is the Heaviside step function. Thus if $b > 0$, g contains only the positive-frequency components of g_0, and if $b < 0$, it contains only the negative-frequency components. In either case, the factor $\mathrm{e}^{-\omega b}$ in the extended Fourier kernel

$$\mathrm{e}^{-\mathrm{i}\omega\tau} = \mathrm{e}^{-\omega b}\mathrm{e}^{-\mathrm{i}\omega t}$$

acts as a *low-pass filter*, substantially damping frequencies $|\omega| \gg b^{-1}$ and thus smoothing out $g(\tau)$. If the driving signal g_0 is assumed *real*, then $\hat{g}_0(\pm\omega)$ are related by complex conjugation and therefore so are $g(t \mp \mathrm{i}b)$. If g_0 is complex, then $\hat{g}_0(\pm\omega)$ are unrelated and so are $g(t \mp \mathrm{i}b)$.

Example. Let $g(\tau)$ be the $(n-1)$st derivative of the Cauchy kernel[2],

$$g(\tau) = C_n(\tau) = (\mathrm{i}\partial_t)^{n-1}\frac{1}{2\mathrm{i}\pi\,\tau} = \frac{(n-1)!}{2\pi\,\mathrm{i}^n\tau^n} \tag{26}$$

[2] The driving signal is the singular distribution $g_0(t) = (\mathrm{i}\partial_t)^{n-1}\delta(t)$, but this can be approximated.

whose Fourier transform is

$$\hat{C}_n(\omega, b) = \int_{-\infty}^{\infty} \mathrm{d}t\, \mathrm{e}^{\mathrm{i}\omega t} C_n(t - \mathrm{i}b) = \mathrm{Sgn}(b)\Theta(\omega b)\omega^{n-1}\, \mathrm{e}^{-\omega b}. \tag{27}$$

Thus, while b acts to suppress high frequencies, $n > 1$ acts to suppress low frequencies and we end up with a *band-pass filter* whose effective centre frequency and bandwidth are given by a Poisson distribution,

$$\omega_n = \frac{n}{b} \qquad \Delta\omega = \frac{\sqrt{n}}{|b|}. \tag{28}$$

The behaviour of Ψ in the far zone is governed by that of $g(\tau - s)$. By (9),

$$C_n(\tau - \sigma) = \frac{(n-1)!}{2\pi \mathrm{i}^n (\tau - \sigma)^n} \approx \frac{(n-1)!}{2\pi[(b - a\cos\theta) + \mathrm{i}(t - r)]^n}$$

is a *pulse* with angle-dependent duration

$$T(\theta) = |b - a\cos\theta| \geqslant |b| - a = T_{\min} > 0 \tag{29}$$

being shortest at $\theta = 0$ if $b > a$ and at $\theta = \pi$ if $b < -a$. While the pulse duration is independent of n, the *strength* of the peak depends jointly on the size of n and the smallness of $b - a$:

$$M(\theta) = |g(\tau - \sigma)|_{t=r} \approx \frac{(n-1)!}{2\pi T(\theta)^n}. \tag{30}$$

To get a measure of the diffraction angle, assume $b > a$ for definiteness. Fix $\beta > 0$ and look for the angle θ_β at which

$$M(\theta_\beta) = \mathrm{e}^{-\beta} M(0).$$

Then

$$(b - a\cos\theta_\beta)^n = \mathrm{e}^{\beta}(b - a)^n$$

which gives

$$2\sin^2(\theta_\beta/2) = 1 - \cos\theta_\beta = (\mathrm{e}^{\beta/n} - 1)\frac{b - a}{a}. \tag{31}$$

Thus, θ_β can be made small either by choosing $b - a \ll a$, or $n \gg \beta$. In either case, the right-hand side gives $\theta_\beta^2/2$. A reasonable measure is obtained with $\beta = 1$.

3. From scalar to vector wavelets

It is well known that every electromagnetic field can be derived from a pair of real scalar potentials, the most well-known examples of which are the *Whittaker* and *Debye* superpotentials [N55]. In this section we use the scalar wavelet Ψ as a *complex* Whittaker superpotential. Although this is equivalent to using a pair of real potentials, disentangling the real and imaginary parts leads to unnecessarily complicated expressions, something like taking the real and imaginary parts of a complicated analytic function $f(x + \mathrm{i}y)$ in order to obtain two real harmonic functions. To see how bad it gets, note from (49) that the fields and currents contain terms of the type $\sigma^{k-3} g^{(k)}(\tau - \sigma)$ with $k = 0, 1, 2$. In the *simplest* case $k = 2$ (which will give the radiation terms of the field), (19) gives

$$\begin{aligned}
\frac{\ddot{g}(\tau - \sigma)}{\sigma} &= \frac{g_1(t - b, b - q) + \mathrm{i}g_2(t - b, b - q)}{p - \mathrm{i}q} \\
\mathrm{Re}\left\{\frac{\ddot{g}(\tau - \sigma)}{\sigma}\right\} &= \frac{p\ddot{g}_1(t - b, b - q) - q\ddot{g}_2(t - b, b - q)}{p^2 + q^2} \\
\mathrm{Im}\left\{\frac{\ddot{g}(\tau - \sigma)}{\sigma}\right\} &= \frac{p\ddot{g}_2(t - b, b - q) + q\ddot{g}_1(t - b, b - q)}{p^2 + q^2}
\end{aligned} \tag{32}$$

and it is clear that the real expressions quickly become unmanageable. Thus, although we work with complex potentials and fields, we view this as a very compact and efficient way of computing the *real* fields. In particular, our expressions contain *nothing extraneous* since their imaginary as well as real parts have a direct physical significance. This strategy is based on the *analyticity* of Ψ outside the source region, which will indeed make *harmonic pairs* out the fields $\boldsymbol{D}$ and $\boldsymbol{B}$, as seen below.

With Ψ as a complex Whittaker superpotential, we define the retarded complex *Hertz potential*

$$\boldsymbol{Z} = \Psi\boldsymbol{\pi} \tag{33}$$

where $\boldsymbol{\pi}$ is a fixed complex *polarization vector* that can be seen [K3] to be a combination of (real) *electric and magnetic dipole moments*. The real and imaginary parts of $\boldsymbol{Z}$

$$\boldsymbol{Z} = \boldsymbol{Z}_e + \mathrm{i}\boldsymbol{Z}_m$$

are interpreted as *electric and magnetic Hertz vectors* [BW99, p 84, 85]. They generate a 4-vector potential A_μ ($\mu = 0, 1, 2, 3$) by

$$A_0 = -\nabla \cdot \boldsymbol{Z}_e \qquad \boldsymbol{A} = \partial_t \boldsymbol{Z}_e + \nabla \times \boldsymbol{Z}_m \tag{34}$$

which automatically satisfies the Lorenz condition

$$\partial_t A_0 + \nabla \cdot \boldsymbol{A} = 0. \tag{35}$$

In turn, it follows from potential theory (or the Poincarè lemma for differential forms) that *every* 4-vector potential satisfying (35) can be written in the form (34), so this representation is quite general. (We can even dispense with the Lorenz condition by performing a gauge transformation on A_μ. See [N55] for an excellent and thorough account of Hertz potentials and their enormous gauge group.) The real vector fields $\boldsymbol{P}_e$ and $\boldsymbol{P}_m$ defined by

$$\boldsymbol{P} = \boldsymbol{P}_e + \mathrm{i}\boldsymbol{P}_m = \Box\,\boldsymbol{Z} = (\Box\,\Psi)\boldsymbol{\pi} = S\boldsymbol{\pi} \tag{36}$$

are the *electric and magnetic polarization densities*. They are distributions supported spatially on the branch cut $\mathcal{B}$. Since we are in Lorenz gauge, the charge-current density is $J_\mu = \Box\, A_\mu$, hence

$$J_0 = -\nabla \cdot \boldsymbol{P}_e \qquad \boldsymbol{J} = \partial_t \boldsymbol{P}_e + \nabla \times \boldsymbol{P}_m \tag{37}$$

with charge conservation guaranteed by the Lorenz condition. The polarization densities thus act as 'potentials' for the charge-current density, a property inherited directly from (34).

The reason why Hertz potentials will be so useful can be seen by computing the fields:

$$\boldsymbol{B} = \nabla \times \boldsymbol{A} = \nabla \times \nabla \times \boldsymbol{Z}_m + \partial_t \nabla \times \boldsymbol{Z}_e \tag{38}$$

and

$$\begin{aligned} \boldsymbol{E} &= -\nabla A_0 - \partial_t \boldsymbol{A} = \nabla\nabla \cdot \boldsymbol{Z}_e - \partial_t^2 \boldsymbol{Z}_e - \partial_t \nabla \times \boldsymbol{Z}_m \\ &= -\Box\,\boldsymbol{Z}_e + \nabla \times \nabla \times \boldsymbol{Z}_e - \partial_t \nabla \times \boldsymbol{Z}_m. \end{aligned} \tag{39}$$

Taking into account (36) gives

$$\boldsymbol{D} = \boldsymbol{E} + \boldsymbol{P}_e = \nabla \times \nabla \times \boldsymbol{Z}_e - \partial_t \nabla \times \boldsymbol{Z}_m \tag{40}$$

which is a kind of 'harmonic conjugate' of (38), so the *real* fields $\boldsymbol{D}, \boldsymbol{B}$ can be expressed compactly in the *complex* form [S41, pp 32–34]

$$\boldsymbol{F} \equiv \boldsymbol{D} + \mathrm{i}\boldsymbol{B} = \nabla \times \nabla \times \boldsymbol{Z} + \mathrm{i}\partial_t \boldsymbol{Z}. \tag{41}$$

Note that outside the branch cut $\mathcal{B}$, $\boldsymbol{P}_e = \boldsymbol{0}$ and $\boldsymbol{D} = \boldsymbol{E}$. The Hertz formalism thus automatically takes account of the polarization, so that the expression (40), if interpreted as a distribution, is valid even within a singular source region.

Again I emphasize that $\boldsymbol{F} = \boldsymbol{D} + \mathrm{i}\boldsymbol{B}$ is 'real' in the sense that $\boldsymbol{D}$ and $\boldsymbol{B}$ are real, physical fields. Yet $\boldsymbol{F}$, like Ψ, is analytic in the source-free complex spacetime region

$$\mathcal{T}_{\mathcal{B}} = \{(\boldsymbol{r} - \mathrm{i}\boldsymbol{a}, t - \mathrm{i}b) \in \mathbb{C}^4 : |b| > a, \boldsymbol{r} \notin \mathcal{B}\}. \tag{42}$$

More simply, because of their spheroidal symmetry, Ψ and $\boldsymbol{F}$ are analytic functions of the two complex variables (σ, τ) in the region

$$\mathcal{U}_{\mathcal{B}} = \{(\sigma, \tau) \in \mathbb{C}^2 : |b| > a, p \neq \chi_{\mathcal{B}}(q)\} \tag{43}$$

where $\chi_{\mathcal{B}}(q)$ is the cut function for $\mathcal{B}$. Thus $\boldsymbol{D}$ and $\boldsymbol{B}$ are really *harmonic conjugates* as suggested earlier. On the other hand, $\boldsymbol{P}$ and J_μ characterize the *singularities* spoiling analyticity in the source region, including the branch points and branch cuts. This differs from the usual practice in the frequency domain, where $(\boldsymbol{D}, \boldsymbol{B})$ are the real parts of separate complex fields $(\boldsymbol{D}_c, \boldsymbol{B}_c)$, and it might appear that these two representations are in conflict since the real fields cannot be extracted by taking the real and imaginary parts of $\boldsymbol{D}_c + \mathrm{i}\boldsymbol{B}_c$. To clarify this, consider the frequency components of $\boldsymbol{F}$,

$$\boldsymbol{F}_\omega = \int_{-\infty}^{\infty} \mathrm{d}t\, \mathrm{e}^{\mathrm{i}\omega t} \boldsymbol{F} = \boldsymbol{D}_\omega + \mathrm{i}\boldsymbol{B}_\omega$$

and note that since $\boldsymbol{F}$ is complex, its positive- and negative-frequency components are *independent*. Therefore a general monochromatic field consists of *two* terms,

$$\begin{aligned} \boldsymbol{G}_{\text{mono}} &= \mathrm{e}^{-\mathrm{i}\omega t} \boldsymbol{F}_\omega + \mathrm{e}^{\mathrm{i}\omega t} \boldsymbol{F}_{-\omega} \qquad \omega > 0 \\ &= \mathrm{e}^{-\mathrm{i}\omega t} (\boldsymbol{D}_\omega + \mathrm{i}\boldsymbol{B}_\omega) + \mathrm{e}^{\mathrm{i}\omega t} (\boldsymbol{D}_{-\omega} + \mathrm{i}\boldsymbol{B}_{-\omega}) \\ &= \mathrm{e}^{-\mathrm{i}\omega t} (\boldsymbol{D}_\omega + \mathrm{i}\boldsymbol{B}_\omega) + \mathrm{e}^{\mathrm{i}\omega t} (\boldsymbol{D}_\omega^* + \mathrm{i}\boldsymbol{B}_\omega^*) \end{aligned}$$

where the reality conditions have been used on $\boldsymbol{D}_\omega$ and $\boldsymbol{B}_\omega$. The representation of a monochromatic field is therefore no different from that of a general field:

$$\boldsymbol{G}_{\text{mono}} = \boldsymbol{D}_{\text{mono}} + \mathrm{i}\boldsymbol{B}_{\text{mono}}$$

with both fields *real*:

$$\boldsymbol{D}_{\text{mono}}(t) = 2\,\mathrm{Re}\{\mathrm{e}^{-\mathrm{i}\omega t} \boldsymbol{D}_\omega\} \qquad \boldsymbol{B}_{\text{mono}}(t) = 2\,\mathrm{Re}\{\mathrm{e}^{-\mathrm{i}\omega t} \boldsymbol{B}_\omega\}.$$

Recall that for $b > a$ and $b < -a$, the analytic signal $g(\tau)$ contains only positive- and negative-frequency components. Therefore

$$b > a \Rightarrow \boldsymbol{D}_\omega + \mathrm{i}\boldsymbol{B}_\omega = \boldsymbol{0}\ \forall\, \omega < 0 \qquad b < -a \Rightarrow \boldsymbol{D}_\omega + \mathrm{i}\boldsymbol{B}_\omega = \boldsymbol{0}\ \forall\, \omega > 0.$$

This shows that the monochromatic components of the electromagnetic wavelets satisfy

$$\boldsymbol{B}_{\text{mono}}(t) = 2\,\mathrm{Re}\{\mathrm{i}\mathrm{e}^{-\mathrm{i}\omega t} \boldsymbol{D}_\omega\} = \boldsymbol{D}_{\text{mono}}(t - \pi/2\omega),$$

so $\boldsymbol{B}$ trails $\boldsymbol{D}$ if $b > a$, and it leads $\boldsymbol{D}$ if $b < -a$. (Recall also that the pulse travels along $\pm\boldsymbol{a}$ if $\pm b > a$.) More generally, the wavelets are *helicity eigenstates* with helicity 1 if $b > a$ and -1 if $b < -a$. This concept applies not only the time-harmonic components but also to general time domain fields [K3a]. As already mentioned, using the analytic combinations of fields also has the great advantage of compactness and simplicity over the alternative of disentangling the real and imaginary parts.

Before launching into the field computations, I want to prepare the way for computing *equivalent currents* on the spheroid $\mathcal{S}_\alpha$ in the coming section. Let us construct this spheroid from the two branch cuts $\mathcal{B}_{\pm\alpha}$ given in (15) and (16). Let us now denote by σ the complex distance with the disc $\mathcal{S}_0$ as branch cut. This will be used as a reference for defining the complex distance functions with $\mathcal{B}_{\pm\alpha}$ as cuts, which we denote by $\sigma_\pm$. Let $V_\pm$ be the volumes bounded by $\mathcal{S}_\alpha^\pm$ together with $\mathcal{S}_0$, so that

$$\partial V_+ = \mathcal{S}_\alpha^+ - \mathcal{S}_0 \qquad \partial V_- = \mathcal{S}_0 - \mathcal{S}_\alpha^-$$

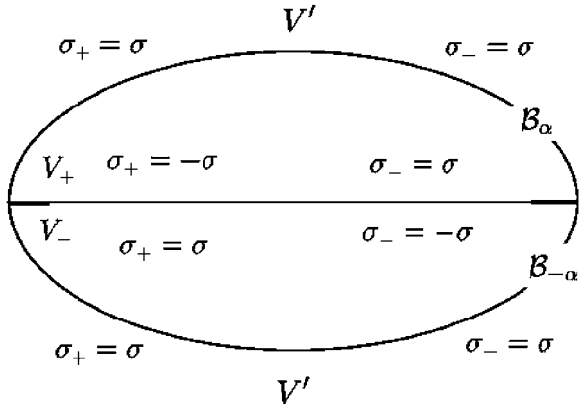

Figure 3. Values of the branches $\sigma_\pm$ of the complex distance function determined by the branch cuts $\mathcal{B}_{\pm\alpha}$, given in terms of the branch σ determined by the disc $\mathcal{S}_0$.

where the signs are related to the *orientations* of $\mathcal{S}_\alpha^\pm$ and $\mathcal{S}_0$ by $\boldsymbol{a}$. The union and compliments of $V_\pm$ will be denoted by

$$V = V_+ \cup V_- \qquad V'_\pm = \mathbb{R}^3 - V_\pm \qquad V' = \mathbb{R}^3 - V.$$

Now recall the rule for crossing a branch cut *other than the reference* cut $\mathcal{S}_0$: $\sigma_\mathcal{B}$ changes sign. Thus, denoting the complex distance functions with respect to $\mathcal{B}_{\pm\alpha}$ by $\sigma_\pm$, we have

$$\sigma_\pm = \begin{cases} \sigma & \text{in} \quad V'_\pm \\ -\sigma & \text{in} \quad V_\pm \end{cases} \tag{44}$$

as shown in figure 3.

The field radiated *jointly* by the two branch cuts $\mathcal{B}_{\pm\alpha}$ is therefore

$$\boldsymbol{F}_\alpha(\sigma,\tau) = \begin{cases} 2\boldsymbol{F}(\sigma,\tau) & \text{in} \quad V' \\ \boldsymbol{F}(-\sigma,\tau) + \boldsymbol{F}(\sigma,\tau) & \text{in} \quad V_+ \\ \boldsymbol{F}(\sigma,\tau) + \boldsymbol{F}(-\sigma,\tau) & \text{in} \quad V_-. \end{cases}$$

Observe that *there is no field discontinuity in going from* V_+ to V_-, *hence*

$$\boldsymbol{F}_\alpha(\sigma,\tau) = \begin{cases} 2\boldsymbol{F}(\sigma,\tau) & \text{in} \quad V' \\ \boldsymbol{F}(-\sigma,\tau) + \boldsymbol{F}(\sigma,\tau) & \text{in} \quad V \end{cases} \tag{45}$$

as depicted in figure 4.

The transition $\sigma \to -\sigma$ across a branch cut turns *retarded* fields into *advanced* fields since

$$\Psi(-\sigma,\tau) = -\frac{g(\tau+\sigma)}{\sigma}. \tag{46}$$

Although advanced fields are usually associated with acausal behaviour, there is a perfectly causal explanation for (46). Consider the field radiated *backward* from $\mathcal{B}_\alpha$, as observed in V_+. Due to the curvature of the back side of $\mathcal{B}_\alpha$, this field *converges* towards the focal ring $\mathcal{C}$ and, having passed though, it is no longer in V_+ and therefore diverges normally. A similar argument explains why the field emitted *forward* from $\mathcal{B}_{-\alpha}$ first converges towards $\mathcal{C}$ and then diverges away from it. The usual acausal behaviour associated with advanced fields is due to the assumption that they *remain* advanced for the indefinite future. (This argument also applies to *time-reversed acoustics* [F0], where time reversal occurs only in a bounded spacetime region.)

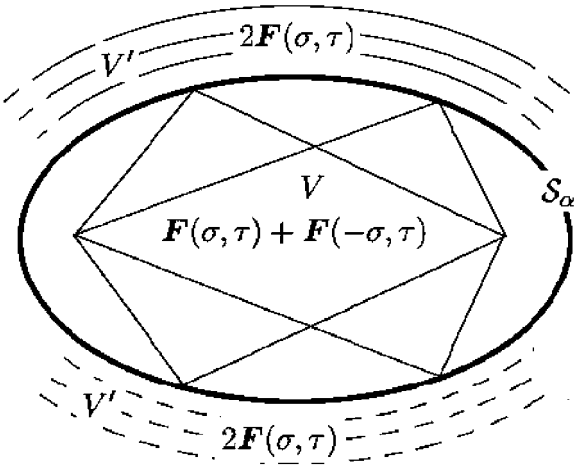

Figure 4. Interior and exterior fields radiated by the oblate spheroid $\mathcal{S}_\alpha$, represented as a combination of the two branch cuts $\mathcal{B}_{\pm\alpha}$.

It was shown in [K3] that the sources of $\Psi(\sigma,\tau)$ and $\Psi(-\sigma,\tau)$ are equal and opposite; that is they form a *source-sink pair*:

$$\Box\,\Psi(-\sigma,\tau) = -\Box\,\Psi(\sigma,\tau) = -S. \tag{47}$$

The proof is trivial for real point sources, where

$$\Box\,\frac{g_0(t\pm r)}{r} = -4\pi g_0(t\pm r)\delta(\boldsymbol{r}) = -4\pi g_0(t)\delta(\boldsymbol{r}).$$

But it is more subtle for complex point sources because the *extended delta function*

$$\tilde{\delta}(\boldsymbol{z}) = -\nabla^2\frac{1}{4\pi\sigma} \qquad \boldsymbol{z} = \boldsymbol{r} - \mathrm{i}\boldsymbol{a}$$

with $\boldsymbol{a}\neq\boldsymbol{0}$ fixed, is not supported at a single point but on the entire branch cut $\mathcal{B}$ and therefore

$$f(\sigma)\tilde{\delta}(\boldsymbol{z}) \neq f(0)\tilde{\delta}(\boldsymbol{z}).$$

In fact, the left-hand side is not even *defined* since σ is discontinuous precisely on the disc supporting $\tilde{\delta}(\boldsymbol{z})$; therefore, some care must be used in proving (47).

Equation (47) shows that the *interior superpotential* $\Psi(\sigma,\tau)+\Psi(-\sigma,\tau)$ *is sourceless, as are the Hertz potentials and electromagnetic fields derived from it*. The interior field is

$$\boldsymbol{F}_0(\sigma,\tau) = \boldsymbol{F}(\sigma,\tau) + \boldsymbol{F}(-\sigma,\tau). \tag{48}$$

Let us first compute the exterior field $\boldsymbol{F}$, which will give the interior field by symmetrizing with respect to σ. Let

$$\Psi' \equiv \partial_\sigma\Psi = -\frac{\dot{g}_r}{\sigma} - \frac{g_r}{\sigma^2} \qquad \dot{g}_r = \partial_t g_r(\tau-\sigma)$$

$$\Psi'' = \partial_\sigma\Psi' = \frac{\ddot{g}_r}{\sigma} + \frac{2\dot{g}_r}{\sigma^2} + \frac{2g_r}{\sigma^3} = \frac{\ddot{g}_r - 2\Psi'}{\sigma}$$

$$\boldsymbol{u} = \nabla\sigma = \nabla p - \mathrm{i}\nabla q = \frac{\boldsymbol{z}}{\sigma}$$

and note that $\boldsymbol{u}$ is a complex unit vector:

$$\boldsymbol{u}\cdot\boldsymbol{u} = \frac{\boldsymbol{z}\cdot\boldsymbol{z}}{\sigma^2} = 1.$$

Thus

$$\nabla \times \boldsymbol{Z} = \nabla\Psi \times \boldsymbol{\pi} = \Psi' \boldsymbol{u} \times \boldsymbol{\pi}$$
$$\nabla \times \nabla \times \boldsymbol{Z} = \Psi'' \boldsymbol{u} \times (\boldsymbol{u} \times \boldsymbol{\pi}) + \Psi' \nabla \times (\boldsymbol{u} \times \boldsymbol{\pi})$$

and by a simple computation,

$$\boldsymbol{u} \times (\boldsymbol{u} \times \boldsymbol{\pi}) = \lambda \boldsymbol{u} - \boldsymbol{\pi} \qquad \lambda = \boldsymbol{u} \cdot \boldsymbol{\pi}$$
$$\nabla \times (\boldsymbol{u} \times \boldsymbol{\pi}) = -\frac{\lambda \boldsymbol{u} + \boldsymbol{\pi}}{\sigma}.$$

Therefore (41) gives

$$\boldsymbol{F} = \Psi''(\lambda \boldsymbol{u} - \boldsymbol{\pi}) - \frac{\Psi'}{\sigma}(\lambda \boldsymbol{u} + \boldsymbol{\pi}) + \mathrm{i}\dot{\Psi}' \boldsymbol{u} \times \boldsymbol{\pi}$$

or

$$\boldsymbol{F} = \left(\frac{\ddot{g}_r}{\sigma} + \frac{3\dot{g}_r}{\sigma^2} + \frac{3g_r}{\sigma^3}\right)\lambda \boldsymbol{u} - \left(\frac{\ddot{g}_r}{\sigma} + \frac{\dot{g}_r}{\sigma^2} + \frac{g_r}{\sigma^3}\right)\boldsymbol{\pi} - \mathrm{i}\left(\frac{\ddot{g}_r}{\sigma} + \frac{3\dot{g}_r}{\sigma^2}\right)\boldsymbol{u} \times \boldsymbol{\pi}. \tag{49}$$

This expression will be written compactly as

$$\boldsymbol{F} = L\lambda \boldsymbol{u} - M\boldsymbol{\pi} - \mathrm{i}N\boldsymbol{u} \times \boldsymbol{\pi} \tag{50}$$

where

$$L = \frac{\ddot{g}_r}{\sigma} + \frac{3\dot{g}_r}{\sigma^2} + \frac{3g_r}{\sigma^3} \qquad M = \frac{\ddot{g}_r}{\sigma} + \frac{\dot{g}_r}{\sigma^2} + \frac{g_r}{\sigma^3} \qquad N = \frac{\ddot{g}_r}{\sigma} + \frac{\dot{g}_r}{\sigma^2}. \tag{51}$$

We now examine the far field to see under what conditions the polarization vector $\boldsymbol{\pi}$ gives the strongest beams. In the far zone (9) we have

$$r \gg a \Rightarrow \sigma \approx r - \mathrm{i}a\cos\theta \qquad \boldsymbol{u} \approx \boldsymbol{e}_r.$$

Therefore

$$\boldsymbol{F}_{\text{far}} = \frac{\ddot{g}(\tau - \sigma)}{r}(\lambda \boldsymbol{e}_r - \boldsymbol{\pi} - \mathrm{i}\boldsymbol{e}_r \times \boldsymbol{\pi})$$
$$= -\frac{\ddot{g}(\tau - \sigma)}{r}(\boldsymbol{\pi}_\perp + \mathrm{i}\boldsymbol{e}_r \times \boldsymbol{\pi}_\perp) \tag{52}$$

where

$$\boldsymbol{\pi}_\perp = \boldsymbol{\pi} - (\boldsymbol{\pi} \cdot \boldsymbol{e}_r)\boldsymbol{e}_r$$

is the component of $\boldsymbol{\pi}$ orthogonal to $\boldsymbol{r}$ which, as expected, is the only one that matters in the far zone. Note that while we have replaced σ by r in the denominator of (52), the presence of $\operatorname{Im}\sigma \approx -r\cos\theta$ in $g(\tau - \sigma)$ plays an *essential* role in determining both the collimation of the beam and the duration of the pulse, as already seen in (30) for $g(\tau) = C_n(\tau)$.

The far field satisfies the *helicity condition*

$$\mathrm{i}\boldsymbol{e}_r \times \boldsymbol{F}_{\text{far}} = \boldsymbol{F}_{\text{far}} \tag{53}$$

or equivalently

$$\boldsymbol{B}_{\text{far}} = \boldsymbol{e}_r \times \boldsymbol{D}_{\text{far}} \qquad \boldsymbol{D}_{\text{far}} = -\boldsymbol{e}_r \times \boldsymbol{B}_{\text{far}}.$$

As we are interested mainly in the paraxial region of the far zone, *the most efficient choice of* $\boldsymbol{\pi}$ *is orthogonal to* $\boldsymbol{a}$. Since

$$\boldsymbol{r} = \boldsymbol{\rho} + z\hat{\boldsymbol{a}} \Rightarrow \boldsymbol{u} = \frac{\boldsymbol{r} - \mathrm{i}\boldsymbol{a}}{\sigma} = \frac{\boldsymbol{\rho}}{\sigma} + \frac{z - \mathrm{i}a}{\sigma}\hat{\boldsymbol{a}}$$

this implies

$$\lambda = \boldsymbol{u} \cdot \boldsymbol{\pi} = \frac{\boldsymbol{\rho} \cdot \boldsymbol{\pi}}{\sigma}.$$

The far-zone energy density is

$$\mathcal{E}_{\text{far}} = \tfrac{1}{2}\{|\boldsymbol{D}_{\text{far}}|^2 + |\boldsymbol{B}_{\text{far}}|^2\} = \tfrac{1}{2}|\boldsymbol{F}_{\text{far}}|^2$$

and, by (53), the far-zone Poynting vector is

$$\boldsymbol{S}_{\text{far}} = \boldsymbol{E}_{\text{far}} \times \boldsymbol{H}_{\text{far}} = \boldsymbol{D}_{\text{far}} \times \boldsymbol{B}_{\text{far}} = \frac{1}{2\text{i}} \boldsymbol{F}^*_{\text{far}} \times \boldsymbol{F}_{\text{far}}$$
$$= \frac{1}{2} \boldsymbol{F}^*_{\text{far}} \times (\boldsymbol{e}_r \times \boldsymbol{F}_{\text{far}}) = \frac{1}{2} |\boldsymbol{F}_{\text{far}}|^2 \boldsymbol{e}_r = \mathcal{E}_{\text{far}} \boldsymbol{e}_r$$

since $\boldsymbol{F}_{\text{far}}$ is orthogonal to $\boldsymbol{e}_r$.

4. Equivalent currents

In principle, the scalar source generates the charge-current density by (36) and (37). But this would involve not only the messy disentangling of the real and imaginary parts of $\boldsymbol{P} = S\boldsymbol{\pi}$ (with both factors complex), but also dealing with the singular nature of S. While S is well defined mathematically as a distribution [K3], it seems to be of little *direct* value from a practical point of view. Since S is supported on the branch cut $\mathcal{B}$, one expects the electromagnetic sources to consist of a surface charge density j_0 and a surface current density $\boldsymbol{j}$. But it turns out that these surface sources are singular on the branch circle $\mathcal{C}$, where $\sigma = 0$. The essence of the problem can be understood from a careful analysis, given in [K1a], of a much simpler case, which we now recall.

Example. The analytically continued Coulomb field due to point charge of strength $Q = 1$ is

$$\boldsymbol{C}(\boldsymbol{r} - \text{i}\boldsymbol{a}) = -\nabla \frac{1}{4\pi\sigma} = \frac{\boldsymbol{r} - \text{i}\boldsymbol{a}}{4\pi\sigma^3}. \tag{54}$$

Newman [N73] has shown that this can be identified with a *real* electromagnetic field $(\boldsymbol{D}, \boldsymbol{B})$ by

$$\boldsymbol{C} = \boldsymbol{D} + \text{i}\boldsymbol{B} \tag{55}$$

interpreted as the flat-spacetime (zero-mass) limit of the Maxwell field in the Kerr–Newman solution in general relativity [N65], which represents a spinning black hole of unit charge[3]. It is instructive to compute the surface sources on a branch cut, which for simplicity we now take to be the disc $\mathcal{S}_0$ defined in (6). On the upper and lower faces of $\mathcal{S}_0$, we have

$$p \to +0 \qquad z \to \pm 0 \qquad \sigma \to \mp\text{i}\sqrt{a^2 - \rho^2}$$

hence

$$\boldsymbol{C} \to \mp \frac{\text{i}\boldsymbol{\rho}}{4\pi(a^2 - \rho^2)^{3/2}} \mp \frac{\boldsymbol{a}}{4\pi(a^2 - \rho^2)^{3/2}}.$$

The jumps in $\boldsymbol{D}$ and $\boldsymbol{B}$ across the cut are therefore

$$\delta\boldsymbol{D} = -\frac{\boldsymbol{a}}{2\pi(a^2 - \rho^2)^{3/2}} \qquad \delta\boldsymbol{B} = -\frac{2\boldsymbol{\rho}}{2\pi(a^2 - \rho^2)^{3/2}}.$$

Since $\delta\boldsymbol{D}$ is orthogonal and $\delta\boldsymbol{B}$ is tangent to $\mathcal{S}_0$, it follows that *the magnetic surface charge- and current-densities vanish as required*. The electric surface densities are given by [J99, p 18]

$$\begin{aligned} j_0 &= -\hat{\boldsymbol{a}} \cdot \delta\boldsymbol{D} = -\frac{a}{2\pi(a^2 - \rho^2)^{3/2}} \\ \boldsymbol{j} &= \hat{\boldsymbol{a}} \times \delta\boldsymbol{B} = -\frac{c\hat{\boldsymbol{a}} \times \boldsymbol{\rho}}{2\pi(a^2 - \rho^2)^{3/2}} = -\frac{c\rho\boldsymbol{e}_\phi}{2\pi(a^2 - \rho^2)^{3/2}} \end{aligned} \tag{56}$$

[3] When $\boldsymbol{D}$ in (55) is reinterpreted as a *Newtonian force field*, then $\boldsymbol{B}$ is a *gravitomagnetic* field related to the 'dragging' of Einsteinian spacetime in the vicinity of a spinning body. Evidently, this effect survives the flat-spacetime limit as the conjugate-harmonic partner to the Newtonian gravitation.

where we have inserted the speed of light (taken earlier to be $c = 1$) for dimensional reasons. Before discussing the problem with (56), note that if we define the *local charge velocity* by

$$\boldsymbol{v} \equiv \frac{\boldsymbol{j}}{\sigma} = \frac{c\rho}{a}\boldsymbol{e}_\phi \tag{57}$$

its linearity in ρ suggests a 'hydrodynamic' interpretation of $\mathcal{S}_0$ as a *rigidly spinning charged disc with angular velocity*

$$\Omega = c/a. \tag{58}$$

In particular, *the rim $\mathcal{C}$ is moving at the speed of light*. While this conclusion seems bizarre in ordinary electrodynamics, it is entirely consistent with the origin of the field $\boldsymbol{C}$ as the residual Maxwell field of a charged, spinning black hole. The investigation in [K1a] has sparked a renewed interest in Newman's original paper [N73], leading to similar interpretations of linearized gravitational fields [N2] and a generalized Lienard–Wiechert field where the radiating point source moves along an arbitrary trajectory in *complex* spacetime [N4]. Our antennas will be similar, but their source is a *dipole* following a complex trajectory and not a monopole, and so their charge-current densities are generated by *polarizations*.

We now come to the main lesson taught by this example. $\boldsymbol{C}$ is an analytic continuation of the Coulomb field of a point source with charge $Q = 1$. If the continuation is to make physical sense, the total charge should remain unchanged. This is contradicted by j_0, which is not only strictly *negative* but whose total charge on $\mathcal{S}_0$ is $-\infty$! To resolve this difficulty, it is necessary to treat the charge-current density as a singular *volume distribution*, just as the scalar source $S = \Box\Psi$ was treated in [K3]. The inhomogeneous Maxwell equations now state that the (volume) charge- and current-density are

$$J_0 = \nabla \cdot \boldsymbol{F} \qquad \boldsymbol{J} = -\partial_t \boldsymbol{F} - \mathrm{i}\nabla \times \boldsymbol{F} \tag{59}$$

while the *homogeneous* Maxwell equations require that J_0 and $\boldsymbol{J}$ be real. Taken as *definitions* of the sources in the sense of generalized functions, it was shown in [K3a] that (59) indeed give a sensible answer. The equivalent surface sources on any spheroid $\mathcal{S}_\alpha$ with $\alpha > 0$ are defined by

$$j_0 = \boldsymbol{e}_p \cdot \delta\boldsymbol{F} \qquad \boldsymbol{j} = -\mathrm{i}\boldsymbol{e}_p \times \delta\boldsymbol{F} \tag{60}$$

where the outgoing unit normal $\boldsymbol{e}_p$ on $\mathcal{S}_\alpha$ is computed in the appendix. These sources are found to be *complex*, which means that they include a *magnetic* charge-current density; the latter vanishes in the limit $\alpha \to 0$, in agreement with the above conclusion. The advantage of using $\alpha > 0$ is that the sources are *smooth and bounded*, with a total charge $Q = 1$ as required. As $\alpha \to 0$, they decompose into *surface sources on the interior* of the disc which coincide with (56), plus *line sources* on the rim $\mathcal{C}$. The line sources carry a total charge of ∞, but when the entire source distribution is treated as a generalized function, it carries the correct total charge $Q = 1$. The problem with (56) is that the jump conditions (using infinitesimal pillboxes and loops) can be applied only on the interior of the disc and not on its boundary $\mathcal{C}$. *A similar argument applies to every branch cut*, showing that caution must be exercised in computing equivalent sources, a lesson we will recall when computing the currents required to produce electromagnetic wavelets.

Finally, we turn to computing the equivalent sources for $\boldsymbol{F}$ on the spheroid $\mathcal{S}_\alpha$. Some important properties of equivalent *real scalar* surface sources were analysed in [HLK0], but their connection to the vector case and, specifically, to our topological use of branch cuts, remains to be explored.

According to (45) and (48), the jump in the field across the spheroid is

$$\delta\boldsymbol{F}(\sigma, \tau) = \boldsymbol{F}(\sigma, \tau) - \boldsymbol{F}(-\sigma, \tau) \tag{61}$$

where the complex distance σ with respect to $\mathcal{S}_0$ is *continuous* across $\mathcal{S}_\alpha$. Unlike the *sum* (48) of retarded and advanced fields, the difference (61) *does* have sources and they are confined to the surface $\mathcal{S}_\alpha$, which we shall presently compute. Begin by writing (50) in the more explicit form

$$\boldsymbol{F}(\sigma,\tau) = L(\sigma,\tau)\lambda\boldsymbol{u} - M(\sigma,\tau)\boldsymbol{\pi} - \mathrm{i}N(\sigma,\tau)\boldsymbol{u}\times\boldsymbol{\pi} \tag{62}$$

with L, M, N given in terms of the *retarded* signal $g_r(\sigma,\tau) = g(\tau-\sigma)$ by

$$L(\sigma,\tau) = \frac{\ddot{g}_r}{\sigma} + \frac{3\dot{g}_r}{\sigma^2} + \frac{3g_r}{\sigma^3} \qquad M(\sigma,\tau) = \frac{\ddot{g}_r}{\sigma} + \frac{\dot{g}_r}{\sigma^2} + \frac{g_r}{\sigma^3} \qquad N(\sigma,\tau) = \frac{\ddot{g}_r}{\sigma} + \frac{\dot{g}_r}{\sigma^2}.$$

Define the *mixed* signals $g_\pm$ by

$$g_\pm(\sigma,\tau) = g(\tau-\sigma) \pm g(\tau+\sigma)$$

and note that

$$\sigma\to-\sigma \Rightarrow \boldsymbol{u} = \frac{\boldsymbol{z}}{\sigma} \to -\boldsymbol{u} \qquad \lambda = \boldsymbol{u}\cdot\boldsymbol{\pi} \to -\lambda.$$

Then we obtain the following expression for the field discontinuity:

$$\delta\boldsymbol{F} = \tilde{L}(\sigma,\tau)\lambda\boldsymbol{u} - \tilde{M}(\sigma,\tau)\boldsymbol{\pi} - \mathrm{i}\tilde{N}(\sigma,\tau)\boldsymbol{u}\times\boldsymbol{\pi} \tag{63}$$

where

$$\tilde{L}(\sigma,\tau) = \frac{\ddot{g}_+}{\sigma} + \frac{3\dot{g}_-}{\sigma^2} + \frac{3g_+}{\sigma^3} \qquad \tilde{M}(\sigma,\tau) = \frac{\ddot{g}_+}{\sigma} + \frac{\dot{g}_-}{\sigma^2} + \frac{g_+}{\sigma^3} \qquad \tilde{N}(\sigma,\tau) = \frac{\ddot{g}_-}{\sigma} + \frac{\dot{g}_+}{\sigma^2}.$$

Before going on to compute the currents, note that (45) can be modified so that the interior field is *any* source-free solution of Maxwell's equations, i.e.,

$$\boldsymbol{F}_\alpha = \begin{cases} 2\boldsymbol{F}(\sigma,\tau) & \text{in} \quad V' \\ \boldsymbol{F}_{\text{int}}(\boldsymbol{r},t) & \text{in} \quad V \end{cases}$$
$$\nabla\cdot\boldsymbol{F}_{\text{int}} = 0 \qquad \mathrm{i}\partial_t\boldsymbol{F}_{\text{int}} = \nabla\times\boldsymbol{F}_{\text{int}}.$$

The choice of an interior solution other than $\boldsymbol{F}_0(\sigma,\tau)$ will, of course, modify the equivalent sources on $\mathcal{S}_\alpha$. However, unless $\boldsymbol{F}_{\text{int}}$ fits into the spheroidal geometry, the resulting sources can be expected to be much more complicated and unnatural, and probably will not benefit from the 'magic' of complex source points. Probably the most general class of interior fields that *do* fit the geometry consists of arbitrary *multiples* of $\boldsymbol{F}_0$, i.e.

$$\boldsymbol{F}_{\text{int}}(\boldsymbol{r},t) = \nu\boldsymbol{F}_0(\sigma,\tau).$$

Then (61) is replaced by

$$\delta\boldsymbol{F}(\sigma,\tau) = \mu\boldsymbol{F}(\sigma,\tau) - \nu\boldsymbol{F}(-\sigma,\tau) \qquad \mu+\nu = 2 \tag{64}$$

and all computations below easily generalize to this case. However, *only when* $\mu = \nu = 1$ *can the radiating surface be interpreted as a combination of branch cuts*! I believe that this case is the most natural and expect it also to be the most useful. For this reason, only it will be treated here, although our results easily extend to the case (64).

I now compute or estimate the various inner and outer products needed in (60). Free use will be made of the results derived in the appendix, and there is no pretense of rigour. I will assume that

$$0 < \alpha \ll a$$

which means that the spheroid is rather *flat*. By (3) and (75),

$$\rho \approx \sqrt{a^2 - q^2} \qquad z = \alpha q \qquad |\nabla p| \approx \frac{a}{|\sigma|} \qquad |\nabla q| \approx \frac{\rho}{|\sigma|}.$$

Thus

$$\boldsymbol{u} = \frac{\boldsymbol{r} - \mathrm{i}\boldsymbol{a}}{\sigma} = \frac{\boldsymbol{\rho} + (z - \mathrm{i}a)\hat{\boldsymbol{a}}}{\sigma} \approx \frac{\boldsymbol{\rho} - \mathrm{i}\boldsymbol{a}}{\sigma}. \tag{65}$$

Recall that $\boldsymbol{\pi}$ is orthogonal to $\boldsymbol{a}$, so that

$$\boldsymbol{\pi} = \pi_\rho \boldsymbol{e}_\rho + \pi_\phi \boldsymbol{e}_\phi$$

and thus

$$\lambda = \boldsymbol{u} \cdot \boldsymbol{\pi} = \frac{\boldsymbol{r} \cdot \boldsymbol{\pi}}{\sigma} = \frac{\boldsymbol{\rho} \cdot \boldsymbol{\pi}}{\sigma} = \frac{\rho \pi_\rho}{\sigma}.$$

From (76) in the appendix, the outgoing unit normal on $\mathcal{S}_\alpha$ is

$$\boldsymbol{e}_p = \frac{\nabla p}{|\nabla p|} = \frac{\alpha \boldsymbol{r} + q\boldsymbol{a}}{\sqrt{\alpha^2 + q^2}\sqrt{\alpha^2 + a^2}} \approx \frac{q\hat{\boldsymbol{a}}}{\sqrt{\alpha^2 + q^2}} = \frac{q}{|\sigma|}\hat{\boldsymbol{a}}. \tag{66}$$

The α^2 term has been retained in the denominator to control the singularity at the equator. (This is the main advantage of using $\mathcal{S}_\alpha$ instead of $\mathcal{S}_0$.) The approximation (66) fails very near the equator $q = 0$, where $\boldsymbol{e}_p$ is far from parallel to $\boldsymbol{a}$, but the analysis in [HLK0] suggests that, for *scalar* wavelets at least, the immediate vicinity of $q = 0$ can be ignored. More precisely, it was shown that for time-harmonic driving signals of frequency ω, the *effective aperture*, emitting most of the radiation, consists of the front surface of the disc $\mathcal{S}_0$ parametrized by

$$k^{-1} \leqslant q \leqslant a \qquad \text{i.e.} \quad \rho^2 \leqslant a^2 - 1/k^2 \qquad k = \omega/c. \tag{67}$$

Of course, this has significance only if $ka > 1$. Lower frequencies generate mostly a reactive field that swirls around the source region and is eventually reabsorbed[4]. Thus, to obtain a high radiation efficiency, it is necessary to use signals $g(\tau)$ with little low-frequency content, such as linear combinations of high-order derivatives of the Cauchy kernel (26). (Of course, a careful repetition of the analysis needs to be made specifically for the electromagnetic case.)

The inner products needed to find j_0 are

$$\begin{aligned}
&\boldsymbol{e}_p \cdot \boldsymbol{u} = \boldsymbol{e}_p \cdot (\nabla p - \mathrm{i}\nabla q) = |\nabla p| \approx \frac{a}{|\sigma|} \\
&\boldsymbol{e}_p \cdot \boldsymbol{\pi} \approx \frac{q}{|\sigma|}\hat{\boldsymbol{a}} \cdot \boldsymbol{\pi} = 0 \\
&\boldsymbol{e}_p \cdot (\boldsymbol{u} \times \boldsymbol{\pi}) = \boldsymbol{\pi} \cdot (\boldsymbol{e}_p \times \boldsymbol{u}) = \boldsymbol{\pi} \cdot (\boldsymbol{e}_p \times (\nabla p - \mathrm{i}\nabla q)) \\
&\qquad\qquad = \mathrm{i}|\nabla q| \boldsymbol{\pi} \cdot (\boldsymbol{e}_q \times \boldsymbol{e}_p) = \mathrm{i}|\nabla q| \boldsymbol{\pi} \cdot \boldsymbol{e}_\phi \approx \frac{\mathrm{i}\rho}{|\sigma|}\pi_\phi.
\end{aligned}$$

The outer products needed for $\boldsymbol{j}$ are

$$\begin{aligned}
&\boldsymbol{e}_p \times \boldsymbol{u} = \mathrm{i}|\nabla q| \boldsymbol{e}_\phi \approx \mathrm{i}\frac{\rho}{|\sigma|}\boldsymbol{e}_\phi \\
&\boldsymbol{e}_p \times \boldsymbol{\pi} \approx \frac{q}{|\sigma|}\hat{\boldsymbol{a}} \times \boldsymbol{\pi} \approx \frac{\mathrm{i}\sigma}{|\sigma|}(\pi_\rho \boldsymbol{e}_\phi - \pi_\phi \hat{\boldsymbol{\rho}}) \\
&\boldsymbol{e}_p \times (\boldsymbol{u} \times \boldsymbol{\pi}) = (\boldsymbol{e}_p \cdot \boldsymbol{\pi})\boldsymbol{u} - (\boldsymbol{e}_p \cdot \boldsymbol{u})\boldsymbol{\pi} \approx -(\boldsymbol{e}_p \cdot \boldsymbol{u})\boldsymbol{\pi} \approx -\frac{a}{|\sigma|}\boldsymbol{\pi}.
\end{aligned}$$

Using these in (60) gives the approximate surface charge density

$$\sigma|\sigma| j_0 \approx \tilde{L} a \rho \pi_\rho + \tilde{N} \sigma \rho \pi_\phi \tag{68}$$

[4] This is consistent with the general fact that 'DC components do not propagate'. It is also the basis of one of the close connections between electromagnetic wavelets and mathematical wavelet theory, since it amounts to an *admissibility condition* on electromagnetic wavelets [K94, p 214].

and the approximate surface current density

$$\sigma|\sigma|\boldsymbol{j} \approx (\tilde{L}\rho^2\pi_\rho - \tilde{M}\sigma^2\pi_\rho + \tilde{N}a\rho\pi_\phi)\boldsymbol{e}_\phi + (\tilde{M}\sigma^2\pi_\phi + \tilde{N}a\sigma\pi_\rho)\boldsymbol{e}_\rho. \tag{69}$$

As expected from our example of the analytic Coulomb potential, the equivalent sources on a spheroid are *complex*, indicating the presence of unrealizable magnetic charges. Since the magnetic sources in that example vanished as $\alpha \to 0$, it is reasonable to hope that this will also be the case here. As the spheroid $\mathcal{S}_\alpha$ with $0 < \alpha \ll a$ is very flat, it may be possible to choose the *phase* of the polarization vector $\boldsymbol{\pi}$ (representing the mixture of electric and magnetic dipoles) so as to minimize the magnetic sources over $\mathcal{S}_\alpha$ excluding the vicinity of the rim $\mathcal{C}$, and the latter region can be ignored for highly oscillatory driving signals as shown in [HLK0]. This question will be addressed in detail elsewhere.

Finally, we compute the *impulse response* of the antenna, i.e. the sources j_μ when the driving signal is the impulse

$$g_0(t) = \delta(t) \Rightarrow g(\tau) = \frac{1}{2\mathrm{i}\pi\tau} = C_1(\tau).$$

Note that the *real* point source version of the scalar wavelet (18) is then the *retarded propagator* for the wave equation,

$$\Psi \to \Psi_0(r,t) = \frac{\delta(t-r)}{r} \qquad \Box\Psi_0 = 4\pi\delta(\boldsymbol{r},t) \tag{70}$$

where the precise relation between Ψ and Ψ_0 is given in terms of complex-distance potential theory in [K3]. The mixed signals are

$$g_+ = \frac{1}{2\mathrm{i}\pi(\tau-\sigma)} + \frac{1}{2\mathrm{i}\pi(\tau+\sigma)} = \frac{\tau}{\mathrm{i}\pi u} \qquad \text{where} \quad u = \tau^2 - \sigma^2$$
$$g_- = \frac{1}{2\mathrm{i}\pi(\tau-\sigma)} - \frac{1}{2\mathrm{i}\pi(\tau+\sigma)} = \frac{\sigma}{\mathrm{i}\pi u}$$

and their time derivatives are

$$\dot{g}_+ = -\frac{\tau^2+\sigma^2}{\mathrm{i}\pi u^2} \qquad \ddot{g}_+ = \frac{2\tau^3+6\tau\sigma^2}{\mathrm{i}\pi u^3}$$
$$\dot{g}_- = -\frac{2\sigma\tau}{\mathrm{i}\pi u^2} \qquad \ddot{g}_- = \frac{6\tau^2\sigma+2\sigma^3}{\mathrm{i}\pi u^3}.$$

This gives

$$\tilde{L} = \frac{15\sigma^4\tau - 10\sigma^2\tau^3 + 3\tau^5}{\mathrm{i}\pi\sigma^3u^3} \qquad \tilde{M} = \frac{9\sigma^4\tau - 2\sigma^2\tau^3 + \tau^5}{\mathrm{i}\pi\sigma^3u^3} \qquad \tilde{N} = \frac{3\sigma^4+6\sigma^2\tau^2-\tau^4}{\mathrm{i}\pi\sigma^2u^3},$$

which can be substituted into (68) and (69) to obtain the impulse response.

In view of the discussion following (67), we are actually more interested in the system's response to the *bandbass signal* in (26),

$$C_n(\tau) = (\mathrm{i}\partial_t)^{n-1}C_1(\tau) = \frac{(n-1)!}{2\pi\mathrm{i}^n\tau^n} = (-\partial_b)^{n-1}C_1(\tau).$$

The induced surface source $j_\mu^{(n)}$ can be computed directly from the impulse response:

$$j_\mu^{(n)} = (-\partial_b)^{n-1}j_\mu. \tag{71}$$

5. Concluding note

Source-free relativistic fields always extend analytically to the double tube domain $\mathcal{T}_{\pm}$ (21) of complex spacetime, as explained in [K3]. I find it quite remarkable that the extension $\Psi(\sigma, \tau)$ of the propagator (70) generates fields with spatially compact sources that are analytic in the source-free parts $\mathcal{T}_{\mathcal{B}}$ of complex spacetime obtained by removing the *world tubes* swept out by the sources. The boundary values of these analytic fields then characterize the singular sources, as shown above.

Acknowledgments

It is a pleasure to thank Drs Richard Albanese, Iwo Bialynicki-Birula, Ehud Heyman, Ted Newman, Ivor Robinson, Andzej Trautman and Arthur Yaghjian for friendly discussions and suggestions related to this work, and David Park for generous help with the figures using his DrawGrahics package. I am especially grateful to Dr Arje Nachman for his sustained support of my research, most recently through AFOSR grant #F49620-01-1-0271.

Appendix

The complex unit vector $\boldsymbol{u}$ is given by

$$\boldsymbol{u} = \nabla\sigma = \frac{\boldsymbol{z}}{\sigma} = \nabla p - \mathrm{i}\nabla q \tag{72}$$

hence

$$\nabla p = \frac{p\boldsymbol{r} + q\boldsymbol{a}}{p^2 + q^2} \qquad \nabla q = \frac{p\boldsymbol{a} - q\boldsymbol{r}}{p^2 + q^2}. \tag{73}$$

Note that

$$\boldsymbol{u}\cdot\boldsymbol{u} = 1 \Rightarrow |\nabla p|^2 - |\nabla q|^2 = 1 \qquad \nabla p \cdot \nabla q = 0 \tag{74}$$

and

$$|\nabla p|^2 + |\nabla q|^2 = \boldsymbol{u}^*\cdot\boldsymbol{u} = \frac{r^2 + a^2}{p^2 + q^2} = \frac{p^2 - q^2 + 2a^2}{p + 2 + q^2}$$

which gives

$$|\nabla p|^2 = \frac{p^2 + a^2}{p^2 + q^2} \qquad |\nabla q|^2 = \frac{a^2 - q^2}{p^2 + q^2}. \tag{75}$$

The unit vectors in the directions of increasing p and q are therefore

$$\boldsymbol{e}_p = \frac{p\boldsymbol{r} + q\boldsymbol{a}}{\sqrt{p^2 + q^2}\sqrt{p^2 + a^2}} \qquad \boldsymbol{e}_q = \frac{p\boldsymbol{a} - q\boldsymbol{r}}{\sqrt{p^2 + q^2}\sqrt{a^2 - q^2}}. \tag{76}$$

References

[BW99] Born M and Wolf E 1999 *Principles of Optics* 7th edn (Cambridge: Cambridge University Press)

[F0] Fink M *et al* 2000 Time-reversed acoustics *Rep. Prog. Phys.* **63** 1933–95

[HF1] Heyman E and Felsen L B 2001 Gaussian beam and pulsed beam dynamics: complex source and spectrum formulations within and beyond paraxial asymptotics *J. Opt. Soc. Am.* **18** 1588–611

[HLK0] Heyman E, Lomakin V and Kaiser G 2000 Physical source realization of complex-source pulsed beams *J. Acoust. Soc. Am.* **107** 1880–91 http://www.wavelets.com/0JASA.pdf

[J99] Jackson J D 1999 *Classical Electrodynamics* 3rd edn (New York: Wiley)

[K94] Kaiser G 1994 *A Friendly Guide to Wavelets* (Boston, MA: Birkhäuser) (6th printing 1999)
[K96] Kaiser G 1996 Physical wavelets and radar: a variational approach to remote sensing *IEEE Antennas Propag. Mag.* **38** 15–24 http://www.wavelets.com/96AP.pdf
[K97] Kaiser G 1997 Short-pulse radar via electromagnetic wavelets *Ultra-Wideband, Short-Pulse Electromagnetics* vol 3 ed C E Baum, L Carin and A P Stone (New York: Plenum) pp 321–6 http://www.wavelets.com/96AMEREM.pdf
[K0] Kaiser G 2000 Complex-distance potential theory and hyperbolic equations *Clifford Analysis* ed J Ryan and W Sprössig (Boston, MA: Birkhäuser) (*Preprint* math-ph/9908031)
[K1] Kaiser G 2001 Communications via holomorphic Green functions *Clifford Analysis and Its Applications* ed F Brackx, J S R Chisholm and V Souček (New York: Plenum) (*Preprint* math-ph/0108006)
[K1a] Kaiser G 2001 Distributional sources for Newman's holomorphic coulomb field Invited paper *Workshop on Canonical and Quantum Gravity III (Warsaw, 7–19 June 2001)* (*Preprint* gr-qc/0108041)
[K3] Kaiser G 2003 Physical wavelets and their sources: real physics in complex spacetime *J. Phys. A: Math. Gen.* **36** R291–R338
[K3a] Kaiser G 2004 Helicity, polarization, and Riemann–Silberstein vortices *J. Opt. A: Pure. Appl. Opt.* **6** S243–S245 (*Preprint* math-ph/0309010)
[N65] Newman E T, Couch E C, Chinnapared K, Exton A, Prakash A and Torrence R 1965 Metric of a rotating, charged mass *J. Math. Phys.* **6** 918–9
[N73] Newman E T 1973 Maxwell's equations and complex Minkowski space *J. Math. Phys.* **14** 102–3
[N2] Newman E T 2002 On a classical, geometric origin of magnetic moments, spin-angular momentum and the Dirac gyromagnetic ratio *Phys. Rev.* D **65** 104005 (*Preprint* gr-qc/0201055)
[N4] Newman E T 2004 Maxwell fields and shear-free null geodesic congruences *Preprint*
[N55] Nisbet A 1955 Hertzian electromagnetic potentials and associated gauge transformations *Proc. R. Soc.* A **231** 250–63
[S41] Stratton J A 1941 *Electromagnetic Theory* (New York: McGraw-Hill)
[SW64] Streater R F and Wightman A S 1964 *PCT, Spin and Statistics, and All That* (Reading, MA: Addison-Wesley)
[W99] Wald R 1999 *Black Holes and Relativistic Stars* (Chicago, IL: University of Chicago Press)

J. Phys. A: Math. Gen. **38** (2005) 495–508 doi:10.1088/0305-4470/38/2/014

Making electromagnetic wavelets: II. Spheroidal shell antennas

Gerald Kaiser

Center for Signals and Waves, 3803 Tonkawa Trail 2, Austin, TX, USA

E-mail: kaiser@wavelets.com

Received 31 August 2004, in final form 5 November 2004
Published 15 December 2004
Online at stacks.iop.org/JPhysA/38/495

Abstract

In the companion paper, a charge–current distribution was obtained for radiating electromagnetic wavelets. However, it cannot be realized because of two drawbacks: (a) it requires the existence of magnetic charges, and (b) the charge–current distribution, which is concentrated on a spheroidal surface $\mathcal{S}_\alpha$, is too singular for practical implementation. Both of these difficulties are resolved here. The first is resolved by using Hertz vectors to generate a charge–current distribution on $\mathcal{S}_\alpha$ due solely to bound electric charges. The second is resolved by replacing $\mathcal{S}_\alpha$ with a spheroidal shell of finite thickness. This generalizes the usual boundary conditions on an interface between electromagnetic media by allowing the transition to be gradual.

PACS numbers: 02.30.Jr, 02.30.Uu, 41.20.Jb, 41.85.Ct

(Some figures in this article are in colour only in the electronic version)

1. Introduction

This paper is aimed at physicists and mathematical physicists interested in classical electrodynamics and optics. In the companion paper [K4], a coherent charge–current distribution for radiating electromagnetic wavelets was constructed on an oblate spheroidal surface $\mathcal{S}_\alpha$. Its main drawback was the necessity of including magnetic along with electric charges, making the sources impossible to realize. Here we show how this difficulty can be overcome by using Hertz vectors [BW99, J99] to generate a charge–current distribution on $\mathcal{S}_\alpha$ due solely to bound electric charges. However, this distribution is still too singular to realize. We show how it can be replaced by a simple volume distribution on a spheroidal shell containing $\mathcal{S}_\alpha$. Our method generalizes the usual boundary conditions on an interface between electromagnetic media by allowing the transition to occur gradually, without incurring additional complexity.

We rely on the concepts in [K4], with some improvements in the notation. For further background on physical wavelets and complex-source pulsed beams, see [K94, HLK0, HF1]. The complex distance from the imaginary source point i$\boldsymbol{a}$ to the real observation point $\boldsymbol{r}$ will be denoted by

$$\tilde{r} = \sqrt{(\boldsymbol{r} - \mathrm{i}\boldsymbol{a}) \cdot (\boldsymbol{r} - \mathrm{i}\boldsymbol{a})} = p - iq \tag{1}$$

and the complex time by

$$\tilde{t} = t - \mathrm{i}b. \tag{2}$$

The imaginary time b plays the role of an overall scale parameter, similar to the scale of ordinary wavelets in one dimension, determining the duration of the pulsed-beam wavelets. The imaginary space vector $\boldsymbol{a}$ similarly controls the spatial extent and orientation of the wavelets. The real and imaginary parts of $\tilde{r}$ satisfy the inequalities

$$|p| \leqslant r, \quad |q| \leqslant a \qquad \text{where} \quad r = |\boldsymbol{r}|, \quad a = |\boldsymbol{a}|. \tag{3}$$

For fixed $\boldsymbol{a} \neq \boldsymbol{0}$, the branch points of $\tilde{r}$ in $\mathbb{R}^3$ form the circle

$$\mathcal{C} = \{\boldsymbol{r} : \tilde{r} = 0\} = \{\boldsymbol{r} : \boldsymbol{a} \cdot \boldsymbol{r} = 0, r = a\}$$

and the 'standard' branch of $\tilde{r}$, defined by $p \geqslant 0$, has for its branch cut the disc

$$\mathcal{D} = \{\boldsymbol{r} : p = 0\} = \{\boldsymbol{r} : \boldsymbol{a} \cdot \boldsymbol{r} = 0, r \leqslant a\}.$$

Here $\tilde{r}$ is real-analytic in $\mathbb{R}^3$ except for a jump discontinuity due to a sign reversal upon crossing $\mathcal{D}$. Every other branch satisfying the positivity condition

$$\boldsymbol{a} \to \boldsymbol{0} \Rightarrow \tilde{r} \to r \geqslant 0$$

can be obtained by continuously deforming $\mathcal{D}$ to a membrane $\mathcal{B}$ with the same boundary,

$$\partial\mathcal{B} = \partial\mathcal{D} = \mathcal{C}.$$

The associated branch of $\tilde{r}$ is defined by

$$\tilde{r}_{\mathcal{B}} = p_{\mathcal{B}} - \mathrm{i}q_{\mathcal{B}} = \begin{cases} \tilde{r}, & \boldsymbol{r} \notin V_{\mathcal{B}} \\ \tilde{r}, & \boldsymbol{r} \in V_{\mathcal{B}} \end{cases} \tag{4}$$

where $V_{\mathcal{B}}$ is the compact volume swept out by deforming $\mathcal{D}$ to $\mathcal{B}$. It follows [K4a] that $\tilde{r}_{\mathcal{B}}$ is real-analytic in $\mathbb{R}^3$ except for a sign reversal across $\mathcal{B}$.

The scalar wavelet[1] with branch cut $\mathcal{B}$ is defined by

$$\Psi_{\mathcal{B}} = \frac{\tilde{g}(\tilde{t} - \tilde{r}_{\mathcal{B}})}{\tilde{r}_{\mathcal{B}}},$$

where $\tilde{g}$ is the ànalytic signal' associated with a driving signal $g(t)$ exciting the source by

$$\tilde{g}(\tilde{t}) = \frac{1}{2\pi\,\mathrm{i}} \int_{-\infty}^{\infty} \frac{g(t')\,\mathrm{d}t'}{\tilde{t} - t'}, \tag{5}$$

which is indeed analytic in the complement of the support of g:

$$\frac{\partial\tilde{g}(\tilde{t})}{\partial\tilde{t}^*} = \frac{1}{2}(\partial_t - \mathrm{i}\partial_b)\tilde{g}(t - \mathrm{i}b) = 0 \qquad \forall\tilde{t} \notin \operatorname{supp} g \subset \mathbb{R}. \tag{6}$$

The significance of the extension parameter b can be understood by noting that the real and imaginary parts of $\tilde{g}$ are

$$g_b(t) = \frac{b}{2\pi} \int_{-\infty}^{\infty} \frac{g(t')\,\mathrm{d}t'}{(t - t')^2 + b^2}, \qquad \hat{g}_b(t) = \frac{1}{2\pi} \int_{-\infty}^{\infty} \frac{(t' - t)g(t')\,\mathrm{d}t'}{(t - t')^2 + b^2}. \tag{7}$$

[1] Strictly speaking, the term 'wavelet' should be reserved for certain choices of g, as explained in [K4]. The scalar wavelet of order n is obtained with $\tilde{g}$ as the nth derivative of the Cauchy kernel $C(\tilde{t}) = 1/2\pi\mathrm{i}\tilde{t}$. Also, note that we use units in which the propagation speed is $c = 1$.

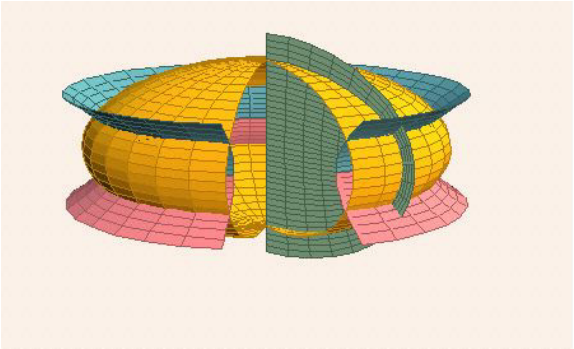

Figure 1. (p, q, ϕ) form an oblate spheroidal coordinate system.

Here g_b is a smoothed version of g with b as the scale or resolution parameter, while $\hat{g}_b$ is a smoothed version of the Hilbert transform of g, again with b as the scale parameter. Thus, time variations of order less than $|b|$ are suppressed in $\tilde{g}(t - \mathrm{i}b)$.

Due to its denominator, $\Psi_{\mathcal{B}}$ is singular on $\mathcal{C}$, where $\tilde{r}_{\mathcal{B}} = 0$, and discontinuous in the interior of $\mathcal{B}$, where $\tilde{r}_{\mathcal{B}}$ reverses sign. To avoid any further singularities, we want to ensure that the numerator $\tilde{g}(\tilde{t} - \tilde{r}_{\mathcal{B}})$ is analytic in all of $\mathbb{R}^3$, and for this it suffices to have its argument bounded away from the real axis by a positive distance. Since

$$\tilde{t} - \tilde{r}_{\mathcal{B}} = t - p_{\mathcal{B}} - \mathrm{i}(b - q_{\mathcal{B}}) \tag{8}$$

and $|q_{\mathcal{B}}| = |q| \leqslant a$, a necessary and sufficient condition is

$$a < |b|. \tag{9}$$

This states that the imaginary spacetime four-vector $(\boldsymbol{a}, b)$ is time-like, belonging to the future cone of spacetime if $a < b$ and the past cone if $b < -a$. The condition (9) will be assumed from now on, making $\Psi_{\mathcal{B}}$ real-analytic in $\mathbb{R}^3 - \mathcal{B}$.

The source $\Sigma_{\mathcal{B}}$ of $\Psi_{\mathcal{B}}$ is defined by applying the wave operator:

$$4\pi\,\Sigma_{\mathcal{B}} = \Box\Psi_{\mathcal{B}} \qquad \text{where} \quad \Box = \partial_t^2 - \Delta. \tag{10}$$

$\Sigma_{\mathcal{B}}$ can be easily shown to vanish wherever $\Psi_{\mathcal{B}}$ is twice differentiable, hence

$$\boldsymbol{r} \notin \mathcal{B} \Rightarrow \Sigma_{\mathcal{B}} = 0. \tag{11}$$

To characterize the source on $\mathcal{B}$, we must apply $\Box$ in a distributional sense [GS64]. Just as differentiating the Heaviside function gives the delta-function, differentiating a discontinuous function like $\Psi_{\mathcal{B}}$ in a distributional sense gives a single layer on the surface of discontinuity, represented by a delta-function of a variable normal to that surface. Since $\Sigma_{\mathcal{B}}$ is obtained by differentiating $\Psi_{\mathcal{B}}$ twice, it will consist of a combination of single and double layers on $\mathcal{B}$ [K4, K4a]. Moreover, these layers diverge on the boundary $\mathcal{C} = \partial\mathcal{B}$ since $\Psi_{\mathcal{B}}$ is singular there. This singularity will be tamed below by combining wavelets with different branch cuts.

The variables (p, q) defined by (1), together with the azimuthal angle ϕ about the $\boldsymbol{a}$-axis, determine an oblate spheroidal coordinate system where the level surfaces of p are the spheroids

$$\mathcal{S}_p: \quad \frac{x^2 + y^2}{p^2 + a^2} + \frac{z^2}{p^2} = 1, \qquad p \neq 0 \tag{12}$$

and the level surfaces of q are the orthogonal hyperboloids $\mathcal{H}_q$. All these quadrics are confocal, having the circle $\mathcal{C}$ as their common focal set. This is depicted in figure 1. As $p \to 0$, $\mathcal{S}_p$ shrinks to a double cover of the disc $\mathcal{D}$.

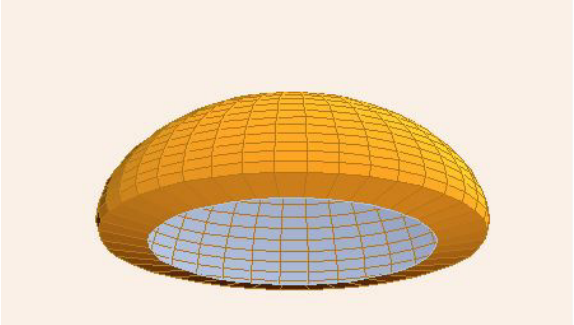

Figure 2. The upper hemispheroidal branch cut $\mathcal{B}_\alpha^+$ with its apron $\mathcal{A}_\alpha$.

When the source of $\Psi_\mathcal{B}$ is computed, it will be singular on $\mathcal{C}$ due to the singularity of $\Psi_\mathcal{B}$ there. In the case of a real point source, this corresponds to the singularity of $\delta(\boldsymbol{r})$ at $\boldsymbol{r} = \mathbf{0}$. Recall that the latter can be regularized by replacing the origin with a sphere of small radius $r = \alpha$, whence $\delta(\boldsymbol{r})$ is replaced by a uniform distribution on the spherical surface. The delta-function can then be defined in terms of the limit $\alpha \to 0$. The equivalent procedure now is to replace the sphere by the oblate spheroid $\mathcal{S}_\alpha$, which is defined by $p = \operatorname{Re}\tilde{r} = \alpha > 0$. But we can go a step further and represent $\mathcal{S}_\alpha$ as a sum of two branch cuts, something that cannot be done for a real point source since the deformation of a point is still a point. Thus, consider the branch cut

$$\mathcal{B}_\alpha^+ = \mathcal{S}_\alpha^+ \cup \mathcal{A}_\alpha \tag{13}$$

consisting of union of the upper hemispheroid

$$\mathcal{S}_\alpha^+ = \{\boldsymbol{r} \in \mathcal{S}_\alpha : z > 0\}$$

and the apron

$$\mathcal{A}_\alpha = \{\boldsymbol{r} : \boldsymbol{r} \cdot \boldsymbol{a} = 0, a^2 \leqslant r^2 \leqslant a^2 + \alpha^2\}$$

connecting $\mathcal{S}_\varepsilon^+$ to the branch circle $\mathcal{C}$, as shown in figure 2. (The apron must be included so that $\partial\mathcal{B}_\alpha^+ = \mathcal{C}$ as required.)

Similarly, let

$$\mathcal{B}_\alpha^- = \mathcal{S}_\alpha^- \cup \mathcal{A}_\alpha \tag{14}$$

be the union of the lower hemispheroid

$$\mathcal{S}_\alpha^- = \{\boldsymbol{r} \in \mathcal{S}_\alpha : z < 0\}$$

with $\mathcal{A}_\alpha$. For simplicity, denote the complex distance with branch cut $\mathcal{B}_\alpha^\pm$ by $\tilde{r}_\pm$ instead of $\tilde{r}_{\mathcal{B}_\alpha^\pm}$ and the corresponding wavelet by $\Psi_\pm$. Let $V_\alpha^\pm$ be the interiors of the upper and lower hemispheroids and V_α be the interior of $\mathcal{S}_\alpha$. According to (4),

$$\begin{aligned}
&\boldsymbol{r} \in V_\alpha^+ \Rightarrow \Psi_+(\tilde{r}, \tilde{t}) = \Psi(-\tilde{r}, \tilde{t}),\ \Psi_-(\tilde{r}, \tilde{t}) = \Psi(\tilde{r}, \tilde{t}) \\
&\boldsymbol{r} \in V_\alpha^- \Rightarrow \Psi_+(\tilde{r}, \tilde{t}) = \Psi(\tilde{r}, \tilde{t}), \quad \Psi_-(\tilde{r}, \tilde{t}) = \Psi(-\tilde{r}, \tilde{t}) \\
&\boldsymbol{r} \notin V_\alpha \Rightarrow \Psi_+(\tilde{r}, \tilde{t}) = \Psi_-(\tilde{r}, \tilde{t}) = \Psi(\tilde{r}, \tilde{t}).
\end{aligned}$$

Consider the average of $\Psi_\pm$,

$$\Psi_A(\tilde{r}, \tilde{t}) = \tfrac{1}{2}\{\Psi_-(\tilde{r}, \tilde{t}) + \Psi_+(\tilde{r}, \tilde{t})\}. \tag{15}$$

Then by the above,

$$\Psi_A(\tilde{r},\tilde{t}) = \begin{cases} \Psi_1(\tilde{r},\tilde{t}), & \boldsymbol{r} \in V_\alpha \\ \Psi_2(\tilde{r},\tilde{t}), & \boldsymbol{r} \notin V_\alpha \end{cases} \tag{16}$$

where the internal field Ψ_1 and the external field Ψ_2 are

$$\Psi_1(\tilde{r},\tilde{t}) = \tfrac{1}{2}\{\Psi(\tilde{r},\tilde{t}) + \Psi(-\tilde{r},\tilde{t})\}, \qquad \Psi_2(\tilde{r},\tilde{t}) = \Psi(\tilde{r},\tilde{t}) \tag{17}$$

and will, for later purposes, be regarded as functions on all of $\mathbb{R}^3$. It follows directly from the definition (5) of $\tilde{g}$ that

$$\begin{aligned} \Psi_1(\tilde{r},\tilde{t}) &= \frac{1}{4\pi \mathrm{i}\tilde{r}} \int_{-\infty}^{\infty} g(t')\,\mathrm{d}t' \left\{ \frac{1}{\tilde{t}-t'-\tilde{r}} - \frac{1}{\tilde{t}-t'+\tilde{r}} \right\} \\ &= \frac{1}{2\pi \mathrm{i}} \int_{-\infty}^{\infty} \frac{g(t')\,\mathrm{d}t'}{(\tilde{t}-t')^2 - \tilde{r}^2}, \end{aligned} \tag{18}$$

which depends only on $\tilde{r}^2$ and is therefore independent of the choice of branch cut. Furthermore, since (9) ensures that

$$|\tilde{t} - t' \pm \tilde{r}| \geqslant |\mathrm{Im}(\tilde{t} - t' \pm \tilde{r})| = |b \pm q| \geqslant |b| - a > 0,$$

we have

$$|(\tilde{t}-t')^2 - \tilde{r}^2| > (|b| - a)^2 > 0 \quad \forall \boldsymbol{r}.$$

This shows that Ψ_1 is real-analytic in $\mathbb{R}^3$, at least if g has compact support or decays sufficiently rapidly to ensure that the integral (18) converges. That is, by taking the average (17) we have managed to cancel the singularities of $\Psi(\pm\tilde{r},\tilde{t})$ on $\mathcal{C}$ as well as their jump discontinuities across $\mathcal{D}$, leaving a field which is analytic in all of $\mathbb{R}^3$ and hence sourceless:

$$\Box\Psi_1(\tilde{r},\tilde{t}) = 0 \quad \forall(\boldsymbol{r},t) \in \mathbb{R}^4.$$

The only region where Ψ_A fails to be analytic is therefore $\mathcal{S}_\alpha$, where it is discontinuous by (16). But even there, the irregularity is mild in the sense that the jump discontinuity

$$\Psi_J(\tilde{r},\tilde{t}) \equiv \Psi_2(\tilde{r},\tilde{t}) - \Psi_1(\tilde{r},\tilde{t}) = \tfrac{1}{2}\{\Psi(\tilde{r},\tilde{t}) - \Psi(-\tilde{r},\tilde{t})\} \tag{19}$$

is bounded—unlike that in any single branch $\Psi_\mathcal{B}$, which is singular on $\mathcal{C}$. Like Ψ_1 and Ψ_2, Ψ_J will be regarded as a field on all of $\mathbb{R}^3$, although for the present we need it only on $\mathcal{S}_\alpha$. The source Σ_A of Ψ_A, defined by

$$4\pi\,\Sigma_A = \Box\Psi_A, \tag{20}$$

is therefore a distribution supported on $\mathcal{S}_\alpha$. By the argument below (10), it consists of a combination of single and double layers on $\mathcal{S}_\alpha$, with the difference that these layers are now bounded since $\mathcal{S}_\alpha$ avoids the singular circle $\mathcal{C}$. Even so, it is not clear that the double layer can be realized in practice. In the next section we replace Ψ_A by a continuous field, where the transition from Ψ_1 to Ψ_2 occurs gradually over a range of spheroids, whose source is supported on a spheroidal shell instead of a single spheroid. (This explains the reason for viewing Ψ_1, Ψ_2 and Ψ_J as fields on all of $\mathbb{R}^3$.) Such volume sources, and their electromagnetic counterparts considered in the following section, should be realizable.

2. Spheroidal shell sources

Let H be the Heaviside step function. Since $0 \leqslant p < \alpha$ in the interior of $\mathcal{S}_\alpha$ and $p > \alpha$ in the exterior, we have

$$\Psi_A = H(\alpha - p)\Psi_1 + H(p - \alpha)\Psi_2. \tag{21}$$

It is natural to use the vector field orthogonal to $\mathcal{S}_p$ given by [K3, appendix]

$$\boldsymbol{n} \equiv \nabla p = \frac{p\boldsymbol{r} + q\boldsymbol{a}}{p^2 + q^2}, \tag{22}$$

which is unnormalized with

$$n^2 \equiv |\boldsymbol{n}|^2 = \frac{p^2 + a^2}{p^2 + q^2} \geqslant 1, \qquad \boldsymbol{n} \cdot \nabla q = 0, \qquad \nabla \cdot \boldsymbol{n} = \frac{2p}{p^2 + q^2}. \tag{23}$$

We can compute the source Σ_A in (20) by using

$$\nabla H(p - \alpha) = -\nabla H(\alpha - p) = H'(p - \alpha)\boldsymbol{n} = \delta(p - \alpha)\boldsymbol{n}. \tag{24}$$

Applying the wave operator gives Σ_A as a combination of terms involving $\delta(p - \alpha)$, interpreted as single layers on $\mathcal{S}_\alpha$, and $\delta'(p - \alpha)$, interpreted as *double layers*. As mentioned above, it is doubtful whether the double layer can be realized in practice, and this will get still worse in the electromagnetic case, where the currents involve one more derivative. Since we are interested in physically realizable sources, we now proceed to modify the above construction. The terms involving $\delta(p - \alpha)$ and $\delta'(p - \alpha)$ are unavoidable as long as the source is confined to the surface $\mathcal{S}_\alpha$. To construct more realistic sources, we now choose a function h that approximates the Heaviside function. A convenient example is

$$h(p) = \frac{1}{\pi}\arg(-p + \mathrm{i}\varepsilon) = \frac{1}{\pi}\,\mathrm{ImLog}(-p + \mathrm{i}\varepsilon), \qquad \varepsilon > 0 \tag{25}$$

which becomes the Heaviside function in the limit as $\varepsilon \to 0$. Note that

$$h'(p) = \frac{\varepsilon}{\pi(p^2 + \varepsilon^2)} \tag{26}$$

is indeed an approximation to the delta-function. But the simple choice (25) has the drawback that h' is not compactly supported, so the resulting source, although extremely small outside a shell of thickness $\mathcal{O}(\varepsilon)$, will not have strictly compact spatial support. To obtain a compactly supported source, we now assume that h has the following properties,

$$h(p) + h(-p) = 1 \quad \text{and} \quad h(p) = \begin{cases} 0, & p \leqslant -\varepsilon \\ 1, & p \geqslant \varepsilon \end{cases} \tag{27}$$

where ε will be assumed fixed with

$$0 < \varepsilon < \alpha, \tag{28}$$

so that $h(p - \alpha)$ vanishes on the disc $\mathcal{D}$ where $p = 0$. Define the regularized version of Ψ_A by replacing H by h in (21),

$$\Psi_A^\varepsilon = h(\alpha - p)\Psi_1(\tilde{r}, \tilde{t}) + h(p - \alpha)\Psi_2(\tilde{r}, \tilde{t}). \tag{29}$$

To simplify the equations, we use the abbreviations

$$h_1(p) = h(\alpha - p), \qquad h_2(p) = h(p - \alpha), \tag{30}$$

so that

$$\Psi_A^\varepsilon = h_1\Psi_1 + h_2\Psi_2 \equiv h_k\Psi_k \tag{31}$$

where the Einstein convention of summing over repeated indices has been used. The source Σ_A^ε of Ψ_A^ε is defined as usual by

$$4\pi\,\Sigma_A^\varepsilon \equiv \Box\Psi_A^\varepsilon. \tag{32}$$

To compute this, note that since (27) implies $h'(-p) = h'(p)$,

$$\begin{aligned}\nabla\Psi_A^\varepsilon &= -h'(\alpha - p)\Psi_1\boldsymbol{n} + h'(p-\alpha)\Psi_2\boldsymbol{n} + h_k\nabla\Psi_k \\ &= h'(p-\alpha)\Psi_J\boldsymbol{n} + h_k\nabla\Psi_k\end{aligned} \tag{33}$$

where Ψ_J, defined as in (19) and given by

$$\begin{aligned}\Psi_J(\tilde r,\tilde t) &= \frac{1}{4\pi\,\mathrm{i}\tilde r}\int_{-\infty}^{\infty} g(t')\,\mathrm{d}t'\left\{\frac{1}{\tilde t - t' - \tilde r} + \frac{1}{\tilde t - t' + \tilde r}\right\} \\ &= \frac{1}{2\pi\,\mathrm{i}\tilde r}\int_{-\infty}^{\infty}\frac{(\tilde t - t')g(t')\,\mathrm{d}t'}{(\tilde t - t')^2 - \tilde r^2},\end{aligned} \tag{34}$$

no longer represents a jump discontinuity of the field since we are not confined to a single spheroid. By the same argument used to show that Ψ_1 is real-analytic in $\mathbb{R}^3$, it follows that Ψ_J is real-analytic in $\mathbb{R}^3$ except for being discontinuous on $\mathcal{D}$ and singular on $\mathcal{C}$ due to the factor $1/\tilde r$. Taking the divergence of (33) gives

$$\Delta\Psi_A^\varepsilon = h''(p-\alpha)\Psi_J n^2 + 2h'(p-\alpha)\nabla\Psi_J\cdot\boldsymbol{n} + h'(p-\alpha)\Psi_J\nabla\cdot\boldsymbol{n} + h_k\nabla\Psi_k.$$

Since $\Psi_J(\tilde r,\tilde t)$ is complex-analytic in $\tilde r$ when $\boldsymbol{r}\notin\mathcal{D}$,

$$p > 0 \Rightarrow \nabla\Psi_J = \Psi_{J'}\nabla\tilde r$$

where the prime denotes the complex derivative with respect to $\tilde r$,

$$\Psi_{J'} = \frac{\partial\Psi_J}{\partial\tilde r} = \frac{1}{2}(\partial_p + \mathrm{i}\partial_q)\Psi_J = \frac{1}{2}\{\Psi'(\tilde r,\tilde t) + \Psi'(-\tilde r,\tilde t)\}. \tag{35}$$

By (23),

$$\nabla\tilde r\cdot\boldsymbol{n} = (\nabla p - \mathrm{i}\nabla q)\cdot\boldsymbol{n} = n^2.$$

Subtracting $\partial_t^2\Psi_A^\varepsilon$ thus gives

$$-4\pi\,\Sigma_A^\varepsilon = h''(p-\alpha)\Psi_J n^2 + 2h'(p-\alpha)\Psi_{J'}n^2 + h'(p-\alpha)\Psi_J\nabla\boldsymbol{n} - h_k\Box\Psi_k.$$

But we have seen that $\Box\Psi_1$ vanishes identically and $\Box\Psi_2$ is supported on $\mathcal{D}$, where $h_2 = 0$ by (27) and (28). Using (23) gives the regularized source

$$\boxed{-4\pi\,\Sigma_A^\varepsilon = h''(p-\alpha)\Psi_J n^2 + \frac{2h'(p-\alpha)}{p^2+q^2}\{(p^2+a^2)\Psi_{J'} + p\Psi_J\}} \tag{36}$$

supported on the spheroidal shell

$$\mathcal{S}_\alpha^\varepsilon = \{\boldsymbol{r} : \alpha - \varepsilon \leqslant p \leqslant \alpha + \varepsilon\}. \tag{37}$$

We emphasize that Σ_A^ε is a smooth volume source that depends only on the 'jump field' Ψ_J. Taking the limit $\varepsilon \to 0$ so that h becomes the Heaviside function gives the source Σ_A consisting of single and double layers on $\mathcal{S}_\alpha$.

3. Maxwell's equations and Hertz potentials

We work with the following complex combinations of electromagnetic fields:

$$\boldsymbol{F} = \boldsymbol{D} + \mathrm{i}\boldsymbol{B} \tag{38}$$

$$\boldsymbol{G} = \boldsymbol{E} + \mathrm{i}\boldsymbol{H} = \boldsymbol{F} - 4\pi\boldsymbol{P} \tag{39}$$

$$\boldsymbol{P} = \boldsymbol{P}_e + \mathrm{i}\boldsymbol{P}_m \tag{40}$$

where the units are Gaussian with $c = 1$, $\boldsymbol{P}_e$ is the electric dipole density, and $\boldsymbol{P}_m$ is the magnetic dipole density. Maxwell's equations take the form

$$\nabla \cdot \boldsymbol{F} = 4\pi\rho \qquad \dot{\boldsymbol{F}} + \mathrm{i}\nabla \times \boldsymbol{G} = -4\pi\boldsymbol{J} \tag{41}$$

where $\dot{\boldsymbol{F}} = \partial_t \boldsymbol{F}$. In the general case of complex charge and current densities

$$\rho = \rho_e + \mathrm{i}\rho_m \qquad \boldsymbol{J} = \boldsymbol{J}_e + \mathrm{i}\boldsymbol{J}_m,$$

equations (41) are equivalent to

$$\begin{aligned} \nabla \cdot \boldsymbol{D} &= 4\pi\rho_e \qquad & \dot{\boldsymbol{D}} - \nabla \times \boldsymbol{H} &= -4\pi\boldsymbol{J}_e \\ \nabla \cdot \boldsymbol{B} &= 4\pi\rho_m \qquad & \dot{\boldsymbol{B}} + \nabla \times \boldsymbol{E} &= -4\pi\boldsymbol{J}_m, \end{aligned} \tag{42}$$

so the imaginary parts $(\rho_m, \boldsymbol{J}_m)$ represent the magnetic charge–current density. Since magnetic monopoles are not observed, we must require

$$\rho_m = 0 \quad \text{and} \quad \boldsymbol{J}_m = \boldsymbol{0}. \tag{43}$$

That is, equation (41) are completely equivalent to the usual Maxwell equations if we add the requirement that $(\rho, \boldsymbol{J})$ is real. We will consider solutions derived from a complex *Hertz potential* consisting of electric and magnetic Hertz vectors [BW99, J99]

$$\boldsymbol{Z} = \boldsymbol{Z}_e + \mathrm{i}\boldsymbol{Z}_m \tag{44}$$

whose source is the polarization,

$$\Box\boldsymbol{Z} = 4\pi\boldsymbol{P}. \tag{45}$$

(For this reason, $(\boldsymbol{Z}_e, \boldsymbol{Z}_m)$ are sometimes called polarization potentials.) The field $\boldsymbol{F}$ is then given in terms of $\boldsymbol{Z}$ by

$$\boldsymbol{F} = \nabla \times \nabla \times \boldsymbol{Z} + \mathrm{i}\nabla \times \dot{\boldsymbol{Z}}, \tag{46}$$

and it follows from (39) and (45) that

$$\begin{aligned} \boldsymbol{G} &= \boldsymbol{F} - \Box\boldsymbol{Z} = \nabla \times \nabla \times \boldsymbol{Z} + \mathrm{i}\nabla \times \dot{\boldsymbol{Z}} + \Delta\boldsymbol{Z} - \ddot{\boldsymbol{Z}} \\ &= \nabla\nabla \cdot \boldsymbol{Z} + \mathrm{i}\nabla \times \dot{\boldsymbol{Z}} - \ddot{\boldsymbol{Z}}. \end{aligned} \tag{47}$$

The real form of equations (45)–(47) is [BW99, pp 84, 85]

$$\begin{aligned} \Box\boldsymbol{Z}_e &= 4\pi\boldsymbol{P}_e & \Box\boldsymbol{Z}_m &= 4\pi\boldsymbol{P}_m \\ \boldsymbol{E} &= \nabla\nabla \cdot \boldsymbol{Z}_e - \nabla \times \dot{\boldsymbol{Z}}_m - \ddot{\boldsymbol{Z}}_e & \boldsymbol{B} &= \nabla \times \nabla \times \boldsymbol{Z}_m + \nabla \times \dot{\boldsymbol{Z}}_e \\ \boldsymbol{H} &= \nabla\nabla \cdot \boldsymbol{Z}_e + \nabla \times \dot{\boldsymbol{Z}}_e - \ddot{\boldsymbol{Z}}_m & \boldsymbol{D} &= \nabla \times \nabla \times \boldsymbol{Z}_e - \nabla \times \dot{\boldsymbol{Z}}_m. \end{aligned}$$

An inspection of the expressions for $\boldsymbol{E}$ and $\boldsymbol{B}$ reveals the meaning of the Hertz potentials as 'superpotentials' from which the four-vector potential $(\Phi, \boldsymbol{A})$ can be derived by

$$\Phi = -\nabla \cdot \boldsymbol{Z}_e \qquad \boldsymbol{A} = \nabla \times \boldsymbol{Z}_m + \dot{\boldsymbol{Z}}_e. \tag{48}$$

In fact, these automatically satisfy the Lorenz condition

$$\dot{\Phi} + \nabla \cdot \boldsymbol{A} = 0,$$

and every four-vector potential satisfying it can be derived from Hertz potentials. The freedom to choose a gauge for $(\Phi, \boldsymbol{A})$, including a non-Lorenz gauge, is part of a much greater gauge freedom in $(\boldsymbol{Z}_e, \boldsymbol{Z}_m)$ [N55, BW99].

According to (46), $\boldsymbol{F}$ is a curl, so by (41) the free charge density vanishes:

$$\rho = 0. \tag{49}$$

Furthermore, (47) gives

$$\nabla \times \boldsymbol{G} = \mathrm{i}\nabla \times \nabla \times \dot{\boldsymbol{Z}} - \nabla \times \ddot{\boldsymbol{Z}} = \mathrm{i}\dot{\boldsymbol{F}},$$

therefore by (41), the free current density also vanishes:

$$\boldsymbol{J} = \boldsymbol{0}. \tag{50}$$

Maxwell's equations (42), written in terms of the microscopic fields $(\boldsymbol{E}, \boldsymbol{B})$, now state that

$$\begin{array}{ll} \nabla \cdot \boldsymbol{B} = 0 & \nabla \times \boldsymbol{E} + \dot{\boldsymbol{B}} = \boldsymbol{0} \\ \nabla \cdot \boldsymbol{E} = 4\pi\rho_b & \nabla \times \boldsymbol{B} - \dot{\boldsymbol{E}} = 4\pi \boldsymbol{J}_b \end{array} \tag{51}$$

where

$$\rho_b = -\nabla \cdot \boldsymbol{P}_e \qquad \boldsymbol{J}_b = \dot{\boldsymbol{P}}_e + \nabla \times \boldsymbol{P}_m \tag{52}$$

represent the bound charge and current densities generated by the variable polarizations $(\boldsymbol{P}_e, \boldsymbol{P}_m)$. The fields derived from Hertz potentials as above are thus due entirely to bound sources[2].

4. Spheroidal electromagnetic antennas

In this section, we construct electromagnetic wavelets from scalar wavelets by turning Ψ into $\boldsymbol{Z}$, then compute their charge–current densities. It is essential that the polarization $\boldsymbol{P}$ defined in (45) have compact spatial support, as it cannot otherwise be realized. There are various ways to turn a scalar solution of the wave equation into a vector solution without increasing the support of its source distribution, the simplest being

$$\boldsymbol{Z} = \boldsymbol{p}\Psi \tag{53}$$

where $\boldsymbol{p}$ is a constant (possibly complex) vector. The polarization is then given by

$$4\pi \boldsymbol{P} = \boldsymbol{p}\Box\Psi = 4\pi \boldsymbol{p}\Sigma, \tag{54}$$

so $\boldsymbol{P}$ and Σ have the same support. Since Σ is a distribution consisting of single and double layers on $\mathcal{D}$, so is $\boldsymbol{P}$. A similar construction applies to the different versions supported on the general branch cut $\mathcal{B}$ and the spheroid $\mathcal{S}_\alpha$. As explained below (24), the layers on $\mathcal{B}$ are singular on $\mathcal{C}$ while those on $\mathcal{S}_\alpha$ are bounded. Even so, the charge–current distributions (52) require one further differentiation, hence they generate a still higher layer with coefficient $\delta''(p - \alpha)$, and it is doubtful whether such distributions can be realized. For this reason, we confine our analysis to volume sources on the spheroidal shell $\mathcal{S}_\alpha^\varepsilon$ (37). Define the Hertz potential

$$\boldsymbol{Z}_A^\varepsilon = \boldsymbol{p}\Psi_A^\varepsilon \tag{55}$$

with Ψ_A^ε as in (29), whose polarization density is

$$\boldsymbol{P}_A^\varepsilon = \boldsymbol{p}\Sigma_A^\varepsilon \tag{56}$$

[2] Free charge–current densities can be added by using stream potentials [N55].

with Σ_A^ε given by (36). If we interpret Σ_A^ε as a scalar density, then (56) suggests an interpretation of $\boldsymbol{p}$ as a (complex) combination of electric and magnetic dipole moments. The charge and current densities on the shell, as given by (52), are

$$\rho_b = -\mathrm{Re}\big\{\nabla\cdot\boldsymbol{P}_A^\varepsilon\big\} = -\,\mathrm{Re}\big\{\boldsymbol{p}\cdot\nabla\Sigma_\alpha^\varepsilon\big\} \tag{57}$$

and

$$\boldsymbol{J}_b = \mathrm{Re}\big\{\dot{\boldsymbol{P}}_A^\varepsilon\big\} + \mathrm{Im}\big\{\nabla\times\boldsymbol{P}_A^\varepsilon\big\} = \mathrm{Re}\big\{\boldsymbol{p}\dot{\Sigma}_A^\varepsilon\big\} - \mathrm{Im}\big\{\boldsymbol{p}\times\nabla\Sigma_A^\varepsilon\big\}. \tag{58}$$

Outside the shell $\mathcal{S}_\alpha^\varepsilon$ the potential $\boldsymbol{Z}_A^\varepsilon$ coincides with $\boldsymbol{Z} = \boldsymbol{p}\Psi$, whose pulsed-beam field $\boldsymbol{F}$ was computed in [K4].

5. Extended Huygens sources

The above suggests an generalization of Huygens sources [Hy99], allowing equivalent sources to be represented on shells instead of surfaces surrounding a bounded source. We present this generalization and compare it to the usual method based on boundary conditions on an interface between electromagnetic media. Let $p(\boldsymbol{r},t)$ be a differentiable function, which will be called a zone function. Fix two numbers $p_1 < p_2$ and consider the time-dependent surfaces and volumes in $\mathbb{R}^3$ defined by

$$\begin{aligned} S_1(t) &= \{\boldsymbol{r} : p(\boldsymbol{r},t) = p_1\}, \qquad & S_2(t) &= \{\boldsymbol{r} : p(\boldsymbol{r},t) = p_2\} \\ V_1(t) &= \{\boldsymbol{r} : p(\boldsymbol{r},t) < p_1\}, \qquad & V_2(t) &= \{\boldsymbol{r} : p(\boldsymbol{r},t) > p_2\}. \end{aligned}$$

Given two electromagnetic fields $(\boldsymbol{F}_1, \boldsymbol{G}_1)$ and $(\boldsymbol{F}_2, \boldsymbol{G}_2)$, with or without sources, we want to construct an interpolated field $(\boldsymbol{F}, \boldsymbol{G})$ so that

$$\begin{aligned} \boldsymbol{F}(\boldsymbol{r},t) &= \begin{cases} \boldsymbol{F}_1(\boldsymbol{r},t), & \boldsymbol{r}\in V_1(t) \\ \boldsymbol{F}_2(\boldsymbol{r},t), & \boldsymbol{r}\in V_2(t) \end{cases} \\ \boldsymbol{G}(\boldsymbol{r},t) &= \begin{cases} \boldsymbol{G}_1(\boldsymbol{r},t), & \boldsymbol{r}\in V_1(t) \\ \boldsymbol{G}_2(\boldsymbol{r},t), & \boldsymbol{r}\in V_2(t). \end{cases} \end{aligned} \tag{59}$$

Choose a differentiable function $h_2(\boldsymbol{r},t)$ such that

$$h_2(\boldsymbol{r},t) = \begin{cases} 0, & \boldsymbol{r}\in V_1(t) \\ 1, & \boldsymbol{r}\in V_2(t) \end{cases} \tag{60}$$

and let

$$h_1(\boldsymbol{r},t) = 1 - h_2(\boldsymbol{r},t).$$

We define the interpolated field as

$$\begin{aligned} \boldsymbol{F}(\boldsymbol{r},t) &= h_k(\boldsymbol{r},t)\boldsymbol{F}_k(\boldsymbol{r},t) \\ \boldsymbol{G}(\boldsymbol{r},t) &= h_k(\boldsymbol{r},t)\boldsymbol{G}_k(\boldsymbol{r},t) \end{aligned} \tag{61}$$

where summations over $k = 1, 2$ are implied, and the jump field

$$\begin{aligned} \boldsymbol{F}_J &= \boldsymbol{F}_2 - \boldsymbol{F}_1 = \boldsymbol{D}_J + \mathrm{i}\boldsymbol{B}_J \\ \boldsymbol{G}_J &= \boldsymbol{G}_2 - \boldsymbol{G}_1 = \boldsymbol{E}_J + \mathrm{i}\boldsymbol{H}_J. \end{aligned} \tag{62}$$

Then, according to (41), the charge density of $(\boldsymbol{F}, \boldsymbol{G})$ is

$$4\pi\rho = \nabla\cdot\boldsymbol{F} = 4\pi h_k\rho_k + \nabla h_2\cdot\boldsymbol{F}_J \tag{63}$$

where

$$4\pi\rho_k = \nabla\cdot\boldsymbol{F}_k, \qquad k = 1, 2 \tag{64}$$

are the charge densities of the prescribed fields. Thus, in addition to the interpolated charge density

$$\rho_I = h_k \rho_k \tag{65}$$

we have a transitional charge density given by

$$4\pi\rho_T = \nabla h_2 \cdot \boldsymbol{F}_J \tag{66}$$

which depends only on the component of the jump field $\boldsymbol{F}_J$ parallel to ∇h_2. According to (60), ρ_T vanishes outside the transition shell

$$V_T(t) = \{\boldsymbol{r} : p_1 \leqslant p(\boldsymbol{r}, t) \leqslant p_2\}. \tag{67}$$

Similarly, the current density is

$$4\pi\boldsymbol{J} = -\dot{\boldsymbol{F}} - \mathrm{i}\nabla \times \boldsymbol{G} = 4\pi h_k \boldsymbol{J}_k - \dot{h}_2 \boldsymbol{F}_J - \mathrm{i}\nabla h_2 \times \boldsymbol{G}_J \tag{68}$$

where

$$4\pi\boldsymbol{J}_k = -\dot{\boldsymbol{F}}_k - \mathrm{i}\nabla \times \boldsymbol{G}_k, \qquad k = 1, 2$$

are the current densities of the prescribed fields. Hence $\boldsymbol{J}$ is the sum of the interpolated current density

$$\boldsymbol{J}_I = h_k \boldsymbol{J}_k \tag{69}$$

and a transitional current density on $V_T(t)$ given by

$$4\pi\boldsymbol{J}_T = -\dot{h}_2 \boldsymbol{F}_J - \mathrm{i}\nabla h_2 \times \boldsymbol{G}_J \tag{70}$$

which depends only on $\boldsymbol{F}_J$ (if h_2 is time dependent) and the component of $\boldsymbol{G}_J$ orthogonal to ∇h_2. The electric and magnetic transitional sources are obtained by taking real and imaginary parts. Assuming h_2 is real, this gives

$$\begin{aligned} 4\pi\rho_T^e &= \nabla h_2 \cdot \boldsymbol{D}_J \qquad & 4\pi\boldsymbol{J}_T^e &= -\dot{h}_2 \boldsymbol{D}_J + \nabla h_2 \times \boldsymbol{H}_J \\ 4\pi\rho_T^m &= \nabla h_2 \cdot \boldsymbol{B}_J \qquad & 4\pi\boldsymbol{J}_T^m &= -\dot{h}_2 \boldsymbol{B}_J - \nabla h_2 \times \boldsymbol{E}_J. \end{aligned} \tag{71}$$

Letting h_2 be complex in $V_T(t)$ makes the transition shell a chiral medium mixing electric and magnetic fields. A further generalization is obtained by replacing h_k with 3×3 matrices (dyadics) $\mathbb{H}_k$ satisfying

$$\mathbb{H}_2(\boldsymbol{r}, t) = \begin{cases} 0, & \boldsymbol{r} \in V_1(t) \\ \mathbb{I}, & \boldsymbol{r} \in V_2(t) \end{cases}, \qquad \mathbb{H}_1(\boldsymbol{r}, t) = \mathbb{I} - \mathbb{H}_2(\boldsymbol{r}, t) \tag{72}$$

where $\mathbb{I}$ is the unit matrix. This makes the transition shell $V_T(t)$ a *non-isotropic* medium as well as chiral if $\mathbb{H}_k$ are complex. See [LSTV94] for a treatment of chiral and non-isotropic media.

Choosing the zone function $p(\boldsymbol{r}, t)$ time dependent thus gives a simple formulation of the transition shell as a moving source, which could be useful in the analysis of radiation by moving objects.

To see how all this relates to Huygens' principle, suppose that we are only given a field $(\boldsymbol{F}_2, \boldsymbol{G}_2)$ whose charge–current density $(\rho_2, \boldsymbol{J}_2)$ is confined to $V_1(t)$, and we want to find an equivalent charge–current density confined to $V_T(t)$ whose radiated field in $V_2(t)$ (but not necessarily elsewhere) is $(\boldsymbol{F}_2, \boldsymbol{G}_2)$. We are free to choose the field $(\boldsymbol{F}_1, \boldsymbol{G}_1)$ in any way that gives vanishing interpolated sources

$$\rho_I = h_k \rho_k = 0, \qquad \boldsymbol{J}_I = h_k \boldsymbol{J}_k = \boldsymbol{0}, \tag{73}$$

since the sources of the interpolated field are then purely transitional and hence confined to $V_T(t)$ as desired. To satisfy (73), it suffices to require that $(\rho_1, \boldsymbol{J}_1)$ be confined to $V_2(t)$.

Thus, choosing any field $(\boldsymbol{F}_1, \boldsymbol{G}_1)$ with sources in $V_2(t)$ and any function h_2 satisfying (60), an equivalent charge–current density on $V_T(t)$ is given by (66) and (70). As $p_1 \to p_2$, $V_T(t)$ becomes S_2 and $(\rho_T, \boldsymbol{J}_T)$ become ordinary Huygens surface sources [Hy99].

The freedom to choose $(\boldsymbol{F}_1, \boldsymbol{G}_1)$ (interpreted as the 'interior field' if $V_1(t)$ is bounded) and h_2 is constrained by the requirement that the magnetic charge–current density must vanish, as detailed below.

Now suppose that $p = p(\boldsymbol{r})$ is time independent, so S_k and V_k are fixed, and choose h_k to be time independent and real. As $p_1 \to p_2$, assume that

$$\lim_{p_1 \to p_2} \nabla h_2(\boldsymbol{r}) = \delta(p(\boldsymbol{r}) - p_2)\boldsymbol{n}(\boldsymbol{r})$$

where $\boldsymbol{n}(\boldsymbol{r})$ is a normal vector field on S_2 pointing into V_2. Then (66) and (70) give

$$\begin{aligned} &\rho_T \to \delta(p(\boldsymbol{r}) - p_2)\sigma \\ &\boldsymbol{J}_T \to \delta(p(\boldsymbol{r}) - p_2)\boldsymbol{K}, \end{aligned} \tag{74}$$

where

$$4\pi\sigma = \boldsymbol{n} \cdot \boldsymbol{F}_J \quad \text{and} \quad 4\pi\boldsymbol{K} = -\mathrm{i}\boldsymbol{n} \times \boldsymbol{G}_J \tag{75}$$

are the surface charge and current densities on S_2, whose real and imaginary parts give the electric and magnetic surface sources:

$$\begin{aligned} 4\pi\sigma_e &= \boldsymbol{n} \cdot \boldsymbol{D}_J & 4\pi\boldsymbol{K}_e &= \boldsymbol{n} \times \boldsymbol{H}_J \\ 4\pi\sigma_m &= \boldsymbol{n} \cdot \boldsymbol{B}_J & 4\pi\boldsymbol{K}_m &= -\boldsymbol{n} \times \boldsymbol{E}_J. \end{aligned} \tag{76}$$

Since magnetic monopoles are not observed, σ_m and $\boldsymbol{K}_m$ must vanish. When $p_1 < p_2$, this may be accomplished if h_2 can be chosen so that

$$\nabla h_2 \cdot \boldsymbol{B}_J = 0, \qquad \nabla h_2 \times \boldsymbol{E}_J = \boldsymbol{0}, \tag{77}$$

which is possible[3] if

$$\boldsymbol{E}_J \cdot \boldsymbol{B}_J = 0 \quad \forall \boldsymbol{r} \in V_T(t). \tag{78}$$

In the limit $p_1 \to p_2$, (77) reduces (76) to

$$\begin{aligned} \boldsymbol{n} \cdot \boldsymbol{D}_J &= 4\pi\sigma_e & \boldsymbol{n} \times \boldsymbol{H}_J &= 4\pi\boldsymbol{K}_e \\ \boldsymbol{n} \cdot \boldsymbol{B}_J &= 0 & \boldsymbol{n} \times \boldsymbol{E}_J &= \boldsymbol{0}, \end{aligned} \tag{79}$$

which are the usual boundary conditions on an interface between two media.

Returning to the general time-dependent setting, consider now an alternative procedure of special interest here. Instead of interpolating two prescribed fields $(\boldsymbol{F}_k, \boldsymbol{G}_k)$, let us interpolate two Hertz potentials $\boldsymbol{Z}_k$:

$$\boldsymbol{Z} = h_k \boldsymbol{Z}_k. \tag{80}$$

As seen, this automatically results in vanishing 'free' sources $\rho = 0$, $\boldsymbol{J} = \boldsymbol{0}$. The polarization is found to be

$$4\pi\boldsymbol{P} = \Box\boldsymbol{Z} = 4\pi h_k \boldsymbol{P}_k + 2\dot{h}_2 \dot{\boldsymbol{Z}}_J - 2(\nabla h_2 \cdot \nabla)\boldsymbol{Z}_J - \boldsymbol{Z}_J \Delta h_2$$

where $4\pi\boldsymbol{P}_k = \Box\boldsymbol{Z}_k$ are the polarizations of the prescribed fields. If

$$\mathrm{supp}\boldsymbol{P}_1 \subset V_2 \quad \text{and} \quad \mathrm{supp}\boldsymbol{P}_2 \subset V_1,$$

then the interpolated polarization $h_k\boldsymbol{P}_k$ vanishes and the polarization is purely transitional on $V_T(t)$:

$$4\pi\boldsymbol{P} = 2\dot{h}_2 \dot{\boldsymbol{Z}}_J - 2(\nabla h_2 \cdot \nabla)\boldsymbol{Z}_J - \boldsymbol{Z}_J \Delta h_2. \tag{81}$$

This generalizes (56), and the bound charge–current densities derived from $\boldsymbol{P}_e$ and $\boldsymbol{P}_m$ via (52) generalize (57) and (58).

[3] Letting V_T be a non-isotropic medium by using $\mathbb{H}_k$ (72) makes it easier to enforce the absence of magnetic monopoles.

6. Conclusions

We have improved on the computation of sources for electromagnetic wavelets given in [K4] in two ways: (a) the spheroidal surface $\mathcal{S}_\alpha$ supporting the sources has been replaced by a spheroidal shell $\mathcal{S}_\alpha^\varepsilon$ supporting smooth volume sources. This eliminates the multiple layers on $\mathcal{S}_\alpha$ which make the sources difficult if not impossible to realize; (b) by deriving the sources from Hertz potentials, we have eliminated the magnetic charge–current density, further facilitating their realizability.

The problem with the magnetic sources in [K4] can be better understood from the current perspective. Let the zone function be $p = \mathrm{Re}\,\tilde{r}$ and S_k, V_k be as above with $0 < p_1 < p_2$. Let the fields $(\boldsymbol{F}_k, \boldsymbol{G}_k)$ be derived from the Hertz potentials

$$\boldsymbol{Z}_k = \boldsymbol{p}\Psi_k, \qquad k = 1, 2$$

with Ψ_k given by (17). Recall that Ψ_k are analytic in $(\tilde{r}, \tilde{t})$ for $p > 0$. Therefore the fields $(\boldsymbol{F}_k, \boldsymbol{G}_k)$ are analytic in $(\tilde{\boldsymbol{r}}, \tilde{t})$ for $\boldsymbol{r} \notin \mathcal{D}$, and

$$\boldsymbol{P}_k = \boldsymbol{0}, \qquad \boldsymbol{G}_k = \boldsymbol{F}_k = \boldsymbol{E}_k + \mathrm{i}\boldsymbol{B}_k \qquad \forall \boldsymbol{r} \notin \mathcal{D}.$$

The jump fields

$$\boldsymbol{F}_J = \boldsymbol{G}_J = \boldsymbol{E}_J + \mathrm{i}\boldsymbol{B}_J$$

are also analytic, as is their polarization scalar [K3a]

$$\boldsymbol{F}_J^2 \equiv \boldsymbol{F}_J \cdot \boldsymbol{F}_J = \boldsymbol{E}_J^2 - \boldsymbol{B}_J^2 + 2\mathrm{i}\boldsymbol{E}_J \cdot \boldsymbol{B}_J. \tag{82}$$

The condition (78) thus requires the imaginary part of an analytic function to vanish for $\boldsymbol{r} \in V_T$, which implies that $\boldsymbol{F}_J^2$ vanishes identically. Although every electromagnetic field must have $\boldsymbol{F}_J^2 \to 0$ in the far zone [B15], fields satisfying $\boldsymbol{F}_J^2 = 0$ globally, called null fields, are rather degenerate. In particular, the electromagnetic wavelet fields are not null and hence cannot fulfil (78). Instead, we have begun with an interpolated Hertz potential (80) and derived bound sources in the transition shell, thus preserving analyticity without invoking the existence of magnetic monopoles.

There is still an unsatisfactory aspect to the polarization (56) and charge–current density (57), (58). Namely, they depend on the fixed vector $\boldsymbol{p}$ and thus do not conform to the spheroidal geometry. This suggests using methods of constructing $\boldsymbol{Z}$ from Ψ other than (53). While (53) is the complex version of Whittaker's potentials [W4], there are alternatives which do not require a fixed polarization vector, such as Debye potentials; see [BD98] for example. Such alternatives will be considered in future work.

Acknowledgments

It is a pleasure to thank Drs Richard Albanese, Grant Erdmann, Sherwood Samn and Arthur Yaghjian for helpful discussions. I am also grateful to Dr Arje Nachman for his sustained support of my research, most recently through AFOSR grant no FA9550-04-1-0139.

Note added. After this paper was finished, I learned from Dr Arthur Yaghjian that a similar formulation of the gradual transition between two electromagnetic media has been developed by Lindell *et al* [LTN0]. The present form is somewhat more general in the following respects. (a) The regions and surfaces are allowed to be time dependent. (b) The derivation of generalized Huygens sources in [LTN0] makes the assumption that one of the prescribed fields vanishes, which we find to be unnecessary. This allows extended Huygens sources on V_T with nonvanishing 'internal' fields.

References

[B15] Bateman H 1915/1955 *The Mathematical Analysis of Electrical and Optical Wave-Motion* (Cambridge/New York: Cambridge University Press/Dover)

[BD98] Bukina E N and Dubovik V M 1998 The gauge freedoms of enlarged Helmholtz theorem and the Neumann–Debye potentials; their manifestation in the multipole expansion of conserved current *Preprint* math-ph/9811011

[BW99] Born M and Wolf E 1999 *Principles of Optics,* 7th edn (Cambridge: Cambridge University Press)

[GS64] Gel'fand I M and Shilov G E 1964 *Generalized Functions, Volume 1: Properties and Operations* (New York: Academic)

[HF1] Heyman E and Felsen L B 2001 Gaussian beam and pulsed beam dynamics: Complex source and spectrum formulations within and beyond paraxial asymptotics *J. Opt. Soc. Am.* **18** 1588–611

[HLK0] Heyman E, Lomakin V and Kaiser G 2000 Physical source realization of complex-source pulsed beams *J. Acoust. Soc. Am.* **107** 1880–91 on line at http://www.wavelets.com/0JASA.pdf

[J99] Jackson J D 1999 *Classical Electrodynamics* 3rd edn (New York: Wiley)

[K94] Kaiser G 1994 *A Friendly Guide to Wavelets* (Boston, MA: Birkhäuser) (sixth printing, 1999)

[K3] Kaiser G 2003 Physical wavelets and their sources: real physics in complex spacetime. Topical Review *J. Phys. A: Math. Gen.* **36** R29–R338

[K3a] Kaiser G 2004 Helicity, polarization, and Riemann-Silberstein vortices *J. Opt. A: Pure Appl. Opt.* **6** S243–S245 (*Preprint* math-ph/0309010)

[K4] Kaiser G 2004 Making electromagnetic wavelets *J. Phys. A: Math. Gen.* **37** 5929–47 (*Preprint* math-ph/0402006)

[K4a] Kaiser G 2004 *Eigenwavelets of the wave equation invited paper (George Mason University Conference Honoring Carlos Berenstein, May 2004)* (*Preprint* math-ph/0408044)

[LSTV94] Lindell I V, Sihvola A H, Tretyakov S A and Viitanen A J 1994 *Electromagnetic Waves in Chiral and Bi-Isotropic Media* (Boston, MA: Artech House)

[LTN0] Lindell I V, Tretyakov S A and Nikoskinen K I 2000 Extended electromagnetic continuity condition and generalized Huygens' principle *Electromagnetics* **20** 233–42

[N55] Nisbet A 1955 Hertzian electromagnetic potentials and associated gauge transformations *Proc. R. Soc.* A **231** 250–63

[W4] Whittaker E T 1904 On an expression of the electromagnetic field due to electrons by means of two scalar potential functions *Proc. Lond. Math. Soc.* **1** 367–72

[Hy99] Hansen T B and Yaghjian A 1999 *Plane-Wave Theory of Time-Domain Fields: Near-Field Scanning Applications* (Piscataway, NJ: IEEE)